Inorganic Chemistry
Cite This: Inorg. Chem. XXXX, XXX, XXX−XXX
Article
pubs.acs.org/IC

Molecular Thorium Compounds with Dichalcogenide Ligands: Synthesis, Structure, ^{77}Se NMR Study, and Thermolysis

Wen Wu,[†] David Rehe,[†] Peter Hrobárik,[*,‡,§] Anna Y. Kornienko,[†] Thomas J. Emge,[†] and John G. Brennan[*,†]

[†]Department of Chemistry and Chemical Biology, Rutgers, the State University of New Jersey, 610 Taylor Road, Piscataway, New Jersey 08854-8087, United States

[‡]Department of Inorganic Chemistry, Faculty of Natural Sciences, Comenius University, SK-84215 Bratislava, Slovakia

[§]Institut für Chemie, Technische Universität Berlin, Strasse des 17. Juni 135, D-10623 Berlin, Germany

Supporting Information

ABSTRACT: A series of dimeric thorium disulfides and diselenides have been prepared with sterically undemanding ancillary ligands. Five complexes, $(py)_6Th_2I_4(\mu_2\text{-}S_2)_2$, $(py)_6Th_2Br_2(SC_6F_5)_2(\mu_2\text{-}S_2)_2$, $(py)_6Th_2I_4(\mu_2\text{-}Se_2)_2$, $(py)_6Th_2I_2(SC_6F_5)_2(\mu_2\text{-}Se_2)_2$, and $(py)_6Th_2Br_2(SC_6F_5)_2(\mu_2\text{-}Se_2)_2$, were isolated in high yields by first reducing mixtures of I_2, $F_5C_6SSC_6F_5$, PhSeSePh, or PhSSPh, and PhSeBr with elemental Th, followed by in situ ligand-based redox reactions with elemental sulfur or selenium. These are the first examples of thorium compounds with bridging dichalcogenide ligands. Attempts to prepare chloride derivatives gave mixtures of $(py)_4ThCl_4$ and either $(py)_6Th_2Cl_2(SC_6F_5)_2(\mu_2\text{-}S_2)_2$ or $(py)_8Th_4Se_4(SePh)_4(SC_6F_5)_4$. All products were characterized by single-crystal and powder X-ray diffraction and IR, UV−visible, and NMR spectroscopy. A computational analysis of experimental ^{77}Se NMR chemical shifts reveals that the solvated dimeric structures with two bridging dichalcogenides are maintained in solution. Thermolysis of $(py)_6Th_2I_4(\mu_2\text{-}Se_2)_2$ leads to reduction of the bridging Se_2^{2-} moieties, oxidation of the I^- ligand, and formation of solid-state $ThSe_2$ and I_2.

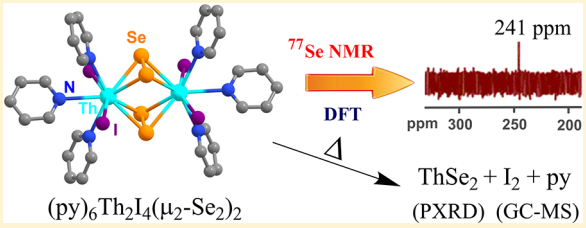

INTRODUCTION

Understanding the complicated nature of bonding in actinide (An) systems remains one of the great challenges in inorganic chemistry, given our incomplete understanding of how much the radially extended 5f orbitals are involved in covalent interactions. In the quest to prepare and characterize appropriately insightful An molecules with significant covalent bonding character, ligands with fewer electronegative chalcogen (E; E = S, Se, Te)-based anions are particularly attractive synthetic targets. Actinide compounds with An−E bonds are also appealing from a reactivity perspective, because these bonds are relatively weak and thus a potential source of controllable reactivity.

Compounds with An−E bonds are found with RE^-,[1] E^{2-},[1b−d,2] and $(E_n)^{2-}$ ligand systems, and of the three, the polychalcogenides (E_n^{2-}, n = 2,[2e−i,3] 3,[1g,2n,3b,4] 4,[2i,5] 5[6]) are the least well developed molecular class. Recent work has explored chemistry with sterically demanding ancillary ligands (i.e., silylamides,[1g,2h,3b−d,7] substituted cyclopentadienyls,[1k−p,2c,k,l,3e,6,8] pyrazolylborates,[1q,r,3f,9] branched alkoxides[1p]), because these ancillaries impart solubility in polar solvents that facilitates crystallization and because their steric bulk inhibits ligand redistribution reactions. Control of steric properties within the primary and secondary coordination sphere in actinide molecules is critical to the preparation of synthetically challenging motifs: i.e., the recent preparation of remarkable compounds with terminal An═E bonds.[3d,7d,10] In contrast, when it becomes interesting to prepare increasingly large polymetallic compounds in order to monitor size-dependent physical properties,[11] sterically demanding ligands can be a liability, and it becomes advantageous to work with sterically undemanding ancillaries.

Polychalcogenide chemistry is particularly attractive because E−E bonds are readily reduced, providing chemists with a potential source of reactivity for rationally building larger clusters or heterometallic compounds. Actinide compounds with E_2^{2-} ligands can be prepared with less congested coordination environments, although success in this area has thus far has been restricted to compounds of uranium. The first example of an actinide molecule with a dichalcogenide ligand was the dioxouranate $UO_2(\text{thiocarbamate})_2(S_2)^{2-}$, prepared by the thermal decomposition of a uranyl thiocarbamate methoxide precursor.[3a] This report was eventually followed by the successful synthesis of $[U(Se_2)_4]^{4-}$,[12] $[UO_2(S_2)_3]^{4-}$,[13] and the imido analogue $[(Bu_2\text{bipyridine})U(NBu)_2I]_2Se_4$.[5]

Related chemistry with thorium is important, because diamagnetic Th(IV) affords an opportunity to probe solution structure, speciation, and reactivity, particularly with compounds of selenium, since the large NMR chemical shift dispersion of ^{77}Se has been useful[3d,14] for correlating solution and solid-state structure/dynamics in both $Th(SeR)_4$ molecules

Received: September 7, 2018

DOI: 10.1021/acs.inorgchem.8b02555
Inorg. Chem. XXXX, XXX, XXX−XXX

and cubane clusters.[1b,s] This work outlines the synthesis and characterization of six dichalcogenido bridged thorium dimers, formed in the ligand-based redox reactions of thorium selenolates with elemental chalcogen. A powerful combination of ^{77}Se NMR and relativistic DFT calculations is used to show that the well-defined solid-state structures are maintained in solution, and an investigation into the thermal decomposition reactions of the halogenated materials shows that ThE_2, rather than ternary solid-state compounds, are produced.

■ EXPERIMENTAL SECTION

General Methods. All syntheses were carried out under ultrapure nitrogen (Welco Praxair), using conventional drybox or Schlenk techniques. Pyridine and hexane (Aldrich) were purified with a dual-column Solv-Tek solvent purification system and collected immediately prior to use. $F_5C_6SSC_6F_5$[15] was prepared according to literature procedures. PhSeSePh (Aldrich) was purchased and recrystallized from hexanes. PhSSPh (Acros), sulfur, selenium, and iodine (Aldrich), thorium chips (International Bioanalytical Industries Inc.), and mercury (Strem Chemicals) were purchased and used as received. Melting points were recorded in sealed capillaries and are uncorrected. IR spectra were recorded on a Thermo Nicolet Avatar 360 FTIR spectrometer from 4000 to 400 cm^{-1} as Nujol mulls on CsI plates. UV−vis absorption spectra were recorded on a Shimadzu UV-3600 double-beam spectrophotometer with the samples dissolved in pyridine. Gas chromatography−mass spectrometry (GC-MS) data were collected on a Varian Saturn 2100T instrument fitted with a capillary column (30 mm length, 0.25 mm i.d., 0.25 mm film thickness). All NMR data were collected on a Varian VNMRS 500 spectrometer at 25 °C with the compounds dissolved in deuterated solvents. ^{1}H and ^{19}F NMR spectra were obtained at 499 and 476 MHz, respectively; ^{77}Se NMR spectra were acquired with a longer relaxation delay (7.0 s) in hydrogen- or fluorine-decoupled mode at 95 MHz using PhSeSePh as an external standard. Elemental analyses were performed by Quantitative Technologies, Inc. (Whitehouse, NJ).

Synthesis of $(py)_6Th_2I_4(S_2)_2$·2py (1). Th (0.232 g, 1.00 mmol), PhSSPh (0.218 g, 1.00 mmol), and I_2 (0.254 g, 1.00 mmol) were combined in pyridine (20 mL) with a catalytic amount of Hg (0.010 g, 0.05 mmol). The mixture was stirred for 12 h until all Th metal was completely consumed to give a yellow solution with trace black powder. Sulfur (0.064 g, 2.00 mmol) and toluene (10 mL) were added, and the mixture was stirred for 1 h to give a yellow solution that was filtered to remove a pale yellow powder, concentrated to 20 mL, and layered with hexanes (15 mL) to form colorless crystals (0.36 g, 46%) that melt at 181 °C and decompose (turn black) at 291 °C. IR: 2924 (w), 2852 (w), 1598 (m), 1463 (m), 1365 (m), 1219 (m), 1151 (w), 1065 (m), 1037 (m), 1002 (m), 738 (s), 695 (s), 623 (s), 542 (m), 466 (w), 417 (m) cm^{-1}. Anal. Calcd for $C_{40}H_{40}I_4N_8S_4Th_2$: C, 27.7; H, 2.33; N, 6.47 (without lattice pyridine $C_{30}H_{30}N_6I_4Th_2S_4$: C, 22.9; H, 1.92; N, 5.34). Found: C, 23.0; H, 2.06; N, 5.24. ^{1}H NMR (toluene-d_8): 8.48 (d, J = 4.8 Hz, 2H, py), 7.00 (m, 1H, py), 6.67 (t, J = 6.0 Hz, 2H, py).

Synthesis of $(py)_6Th_2Br_2(SC_6F_5)_2(S_2)_2$ (2). Th (0.232 g, 1.00 mmol), PhSSPh (0.109 g, 0.50 mmol), $F_5C_6SSC_6F_5$ (0.199 g, 0.50 mmol), and PhSeBr (0.236 g, 1.00 mmol) were combined in pyridine (10 mL) with a catalytic amount of Hg (0.010 g, 0.05 mmol), and the mixture was stirred for 12 h until the thorium metal was completely consumed to give a yellow solution. Sulfur (0.064 g, 2.00 mmol) and toluene (10 mL) were added, and the mixture was stirred for an additional 30 min. The bright yellow solution was filtered to remove a light gray powder, concentrated to 15 mL, and layered with hexanes (15 mL) to give colorless crystals (0.29 g, 36%) that melt at 213 °C and decompose at 273 °C. IR: 2924 (s), 2854 (s), 1630(w), 1601 (m), 1462 (s), 1365 (s), 1261 (m), 1222 (m), 1153 (w), 1079 (w), 1037 (w), 967 (s), 859 (s), 801(s), 741 (s), 694 (s), 624 (m), 578 (w), 482 (w), 419 (w) cm^{-1}. Anal. Calcd for $C_{42}H_{30}N_6Th_2F_{10}Br_2S_6$: C, 31.0; H, 1.86; N, 5.17. Found: C, 31.0; H, 1.91; N, 5.17. ^{1}H NMR (toluene-d_8): 8.54 (broad, 2H, py), 6.94 (m, 1H, py), 6.64 (m, 2H, py). ^{19}F NMR (toluene-d_8): −138 (m, 2F), −159 (t, 1F), −162 (m, 2F).

Synthesis of $(py)_6Th_2Cl_2(SC_6F_5)_2(S_2)_2$ (3). Th (0.232 g, 1.00 mmol), PhSSPh (0.109 g, 0.50 mmol), $F_5C_6SSC_6F_5$ (0.199 g, 0.50 mmol), and PhSeCl (0.192 g, 1.00 mmol) were combined in pyridine (10 mL) with a catalytic amount of Hg (0.010 g, 0.05 mmol), and the mixture was stirred for 12 h until the thorium metal was completely consumed to give a pale yellow solution. Sulfur (0.064 g, 2.00 mmol) and toluene (10 mL) were added, and the mixture was stirred for an additional 45 min. The yellow solution was filtered to remove a light gray powder, concentrated to 15 mL, and layered with hexanes (15 mL) to give colorless crystals, one of which was identified by single-crystal diffraction as $(py)_6Th_2Cl_2(SC_6F_5)_2(S_2)_2$·1.5py (**3**). PXRD of the powdered product revealed that this reaction cocrystallizes as a number of products, including **3** and monomeric $(py)_4ThCl_4$ (**7**).

Synthesis of $(py)_6Th_2I_4(Se_2)_2$·2py (4). Th (0.232 g, 1.00 mmol), PhSeSePh (0.312 g, 1.00 mmol), and I_2 (0.254 g, 1.00 mmol) were combined in pyridine (20 mL) with a catalytic amount of Hg (0.010 g, 0.05 mmol). The mixture was stirred for 12 h until the thorium metal was consumed to give a yellow solution and trace black powder. Elemental selenium (0.158 g, 2.00 mmol) was added, and the mixture was stirred for an additional 30 min. The yellow solution was filtered, concentrated to 10 mL, and layered with hexanes (15 mL) to form yellow crystals (0.53 g, 61%) that melt at 252 °C and decompose (turn black) at 384 °C. IR: 2924 (s), 2853 (s), 1598 (w), 1463 (m), 1365 (s), 1261 (w), 1220 (w), 1067 (w), 1037 (w), 801 (m), 722 (w), 700 (w), 489 (w) cm^{-1}. UV−vis: this compound shows an absorption plateau at ca. 440 nm, but a well-defined maximum was not observed (see Figure S22 in the Supporting Information). Anal. Calcd for $C_{40}H_{40}N_8Th_2I_4Se_4$: C, 25.0; H, 2.10; N, 5.84 (lattice pyridine removed $C_{30}H_{30}N_6Th_2I_4Se_4$: C, 20.5; H, 1.72; N, 4.77). Found: C, 25.1; H, 2.29; N, 5.64. ^{1}H NMR (benzene-d_6): 8.98 (broad, 2H, py), 6.88 (m, 1H, py), 6.62 (m, 2H, py). ^{77}Se NMR (pyridine-d_5): 241 (s).

Synthesis of $(py)_6Th_2I_2(SC_6F_5)_2(Se_2)_2$·py (5). Th (0.232 g, 1.00 mmol), PhSeSePh (0.312 g, 1.00 mmol), $F_5C_6SSC_6F_5$ (0.199 g, 0.50 mmol), and I_2 (0.127 g, 0.50 mmol) were combined in pyridine (20 mL) with a catalytic amount of Hg (0.010 g, 0.05 mmol), and the mixture was stirred for 12 h until the metal was completely consumed to give a yellow solution. Elemental selenium (0.158 g, 2.0 mmol) was added, and the mixture was stirred for 1 h. The pale orange solution was filtered, concentrated to 15 mL, and layered with hexanes (15 mL) to give orange crystals (0.30 g, 31%) that became deep orange and melt at 181 °C and decompose at 290 °C. IR: 2924 (s), 2854 (s), 1601 (w), 1460 (s), 1376 (s), 1261 (w), 1221(w), 1152 (w), 1038 (w), 969 (m), 859 (w), 833 (w), 802 (w), 722 (m), 698 (w), 623 (w) cm^{-1}. UV−vis: this compound shows an absorption plateau at ca. 400 nm. Anal. Calcd for $C_{47}H_{35}N_7Th_2F_{10}I_2S_2Se_4$: C, 28.4; H, 1.78; N, 4.94 (lattice pyridine removed $C_{42}H_{30}N_6Th_2F_{10}I_2S_2Se_4$: C, 26.5; H, 1.59; N, 4.41). Found: C, 28.2; H, 1.97; N, 4.47. ^{1}H NMR (toluene-d_8): 8.71(broad, 2H, py), 6.91 (m, 1H, py), 6.63 (m, 2H, py). ^{19}F NMR (toluene-d_8): −138 (d, 2F), −159 (t, 1F), −162 (m, 2F). ^{77}Se NMR (pyridine-d_5): 332 (s).

Synthesis of $(py)_6Th_2Br_2(SC_6F_5)_2(Se_2)_2$·2py (6). Th (0.232 g, 1.00 mmol), PhSeSePh (0.156 g, 0.50 mmol), $F_5C_6SSC_6F_5$ (0.199 g, 0.50 mmol), and PhSeBr (0.236 g, 1.00 mmol) were combined in pyridine (20 mL) with a catalytic amount of Hg (0.010 g, 0.05 mmol), and the mixture was stirred for 12 h until the thorium metal was consumed to give a yellow solution. Elemental selenium (0.158 g, 2.00 mmol) was added, and the mixture was stirred for an additional 10 min. The pale orange solution was filtered, concentrated to 15 mL, and layered with hexanes (10 mL) to give orange crystals (0.40 g, 44%) that melt at 145 °C and decompose at 416 °C. IR: 2923 (s), 2854 (s), 1601 (m), 1503 (w), 1463 (s), 1376 (s), 1262 (w), 1221 (m), 1151 (w), 1079 (w), 1069 (w), 1038 (m), 1003 (m), 969 (m), 860 (s), 752 (m), 698 (s), 623 (s) cm^{-1}. Anal. Calcd for $C_{52}H_{40}F_{10}Br_2N_8S_2Se_4Th_2$: C, 31.7; H, 2.05; N, 5.69 (lattice pyridine removed $C_{42}H_{30}F_{10}Br_2N_6S_2Se_4Th_2$: C, 27.83; H, 1.67; N, 4.64). Found: C, 31.6; H, 2.11; N, 5.63. ^{1}H NMR (toluene-d_8): 8.72 (broad,

DOI: 10.1021/acs.inorgchem.8b02555
Inorg. Chem. XXXX, XXX, XXX−XXX

2H, py), 6.89 (broad, 1H, py), 6.58 (broad, 2H, py). ^{19}F NMR (toluene-d_8): −138(m, 2F), −159 (t, 1F), −162 (m, 2F). ^{77}Se NMR (pyridine-d_5): 309 (s).

Attempt To Prepare $(py)_6Th_2Cl_2(SC_6F_5)_2(Se_2)_2$. Th (0.232 g, 1.00 mmol), PhSeSePh (0.156 g, 0.50 mmol), $F_5C_6SSC_6F_5$ (0.199 g, 0.50 mmol), and PhSeCl (0.192 g, 1.00 mmol) were combined in pyridine (15 mL) with a catalytic amount of Hg (0.010 g, 0.05 mmol), and the mixture was stirred for 12 h until the metal was completely consumed to give an orange solution. Elemental selenium (0.158 g, 2.00 mmol) was added, and the mixture was then stirred for 10 min. The pale orange solution was filtered, concentrated to 15 mL, and layered with hexanes (15 mL) to give crystals that were ground and identified by PXRD as a mixture of the $(py)_4ThCl_4$ (**7**) and $(py)_8Th_4Se_4(SePh)_4(SC_6F_5)_4$.[1b]

Computational Details. All structures were fully optimized at the PBE0 level of theory,[16] including an atom-pairwise correction for dispersion forces via Grimme's D3 model[17] with Becke-Johnson (BJ)[18] damping in the Turbomole program.[19] Quasirelativistic energy-consistent small-core pseudopotential (effective-core potential, ECP)[20] along with corresponding Gaussian-type orbital valence basis sets of def2-TZVP quality were used for metals (Th, Hf, Zr) and iodine, respectively, while all other atoms were treated with an all-electron def2-TZVP basis set.[21] Relativistic all-electron DFT calculations of the nuclear shielding were performed using the Amsterdam Density Functional (ADF) program suite,[22] employing a customized PBE0 exchange-correlation functional with 40% exact-exchange admixture (PBE0-40HF)[23] in conjunction with Slater-type orbital basis sets of triple-ζ doubly polarized (TZ2P) quality. An integration accuracy of 5 was used. Both scalar and spin−orbit relativistic effects were treated by the two-component zeroth-order regular approximation (ZORA).[24] Bulk solvent effects were simulated by the conductor-like screening model (COSMO)[25] as implemented self-consistently in ADF, considering pyridine as the solvent. The computed ^{77}Se nuclear shieldings were converted to chemical shifts (δ, in ppm) relative to the shielding of Me_2Se, computed at the same level. Where applicable, the calculated shieldings were averaged over the magnetically equivalent nuclei. QTAIM (quantum theory of atoms in molecules) delocalization indices (DI) were evaluated at the ZORA scalar relativistic PBE0/TZ2P level using utilities implemented in the ADF package.[22] The DI integrates the electron density in the bonding region between two atoms in question and serves thus as a quantitative descriptor of the bond covalency.[3d,26] The ADF code was also used for energy decomposition analysis (EDA)[27] of the total bonding energy into steric and electronic (attractive orbital) interactions and for time-dependent DFT calculations of excitation energies.

Thermolysis. A ground sample of **4** (ca. 200 mg) was placed in a quartz thermolysis tube under a nitrogen atmosphere; the tube was evacuated and purged with argon three times, sealed under vacuum, and placed into a Model 847 Lindberg tube furnace. The initially empty "cold" end of the glass tube was held at −196 °C by immersion in liquid nitrogen. The sample was heated to 850 °C at a ramp rate of 10 °C/min and then held at 850 °C for 6 h, at which time it was cooled to 25 °C at a rate of 3.5 °C/min. The gray-black powder that was formed at the sample end of the quartz tube was placed in a glass capillary and identified as $ThSe_2$[10] by PXRD (space group *Pmnb* (No. 62), Z = 4, PDF# 74-0978). GC-MS analysis of the volatile products identified py (m/z 79) and I_2 (m/z 253.8).

Scanning Electron Microscopy (SEM). Field-emission scanning electron microscopy (FE-SEM, ZEISS Sigma) and energy-dispersive X-ray spectroscopy (EDS, silicon drift detector from Oxford Instruments) were employed to record the morphological characteristics of the pyrolysis materials. Imaging and EDS were completed using 5 and 15 keV electron beam voltages, respectively. All samples were covered with a 20 nm Au coating using a rotary-pumped sputter coating system (EMS150R, Electron Microscopy Sciences) and placed on carbon adhesive tape with a specimen holder (Ted Pella).

Polycrystalline X-ray Diffraction (PXRD). PXRD data for compounds **1**−**4**, **6**, and **7** were obtained with a Bruker Vantec-500 area detector and a Bruker FR571 rotating-anode X-ray generator operating at 40 kV and 50 mA and equipped with a three-circle Azlan goniometer. The system used 1.0 mm pinhole collimation and a Rigaku Osmic parallel-mode (e.g., primary beam dispersion less than 0.01° in 2θ) mirror monochromator (Cu Kα; λ = 1.5418 Å). Data were collected at room temperature (20 °C) with a sample to detector distance of approximately 32 cm. Spatial calibration and flood-field correction for the area detector were performed prior to data collection. The 2048 × 2048 pixel images were collected at a fixed detector (2θ) angle of 15° for approximately 10 min with ω fixed and with continuous rotation in ϕ (capillary axis) of about 1°/s. For the intensity versus 2θ plots (see the Supporting Information),[28] background levels, modeled as amorphous scattering from air, capillary, and sample, were subtracted and integrations in χ (Bruker GADDS)[29] were performed. No other corrections to the PXRD data were made. PXRD patterns of ground samples were compared with the calculated diffraction pattern of the respective compound. To account for the temperature difference in the PXRD (T = 293 K) and single-crystal (T = 120 K) patterns, a wavelength of 1.51 Å was used for the calculated PXRD patterns. In addition, it appeared that the intensity and d spacings of low-angle PXRD data were much less affected by evaporation of lattice solvent. Thus, the 4° < 2θ < 12° PXRD data provided an excellent region for the phase verification performed here. Diagrams of the PXRD data are available in the Supporting Information.

Single-Crystal X-ray Structure Determination. Data for **1**−**7** were collected on a Bruker Smart APEX CCD diffractometer with graphite-monochromated Mo Kα radiation (λ = 0.71073 Å) at 120 K.[30] Crystals were immersed in Paratone oil and examined at low temperatures. The data were corrected for Lorentz effects, polarization, and absorption, the last by a face-based numerical method.[30] The structures were solved by direct methods.[31] All non-hydrogen atoms were refined[31] on the basis of F_o^2. All hydrogen atom coordinates were calculated with idealized geometries. All structures were drawn using the Mercury 3.8 program.[32] Crystallographic data and final R indices for **1**−**7** are given in Table S1 of the Supporting Information. The CIF files for **1**−**7** have been deposited with the Cambridge Structural Database with CCDC numbers 1853617−1853623, respectively. Thermal ellipsoid diagrams for **1**−**6** are shown in Figures 1 and 2, and the thermal ellipsoid diagram for **7** is shown in Figure S26. Complete crystallographic details for **1**−**7** are given in the Supporting Information.

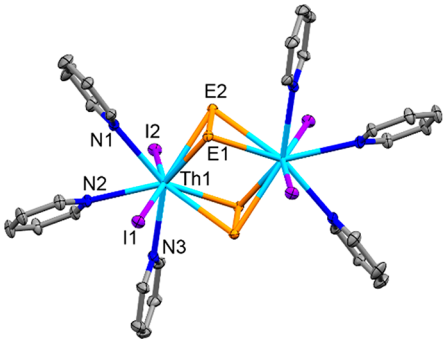

Figure 1. Thermal ellipsoid (ORTEP) diagram of $(py)_6Th_2I_4(E_2)_2$, where E = S (**1**), Se (**4**). Orange denotes S or Se, purple I, light blue Th, dark blue N, and gray C. H atoms are removed for clarity, and ellipsoids are at the 50% probability level. Significant bond length averages are given in Table 1.

RESULTS AND DISCUSSION

Ligand-based redox reactions of thorium halide/chalcogenolates with elemental E give high yields of bimetallic thorium compounds with bridging $(E_2)^{2-}$ ligands. Addition of elemental E to solutions of "$ThI_n(EPh)_{4-n}$" or "$ThX_n(SC_6F_5)_m(EPh)_{4-(n+m)}$" (E = S, Se; X = I, Br, and n = 1−4) leads to the reduction of E to give $(E_2)^{2-}$, oxidation of EPh^- to give PhEEPh, and the formation

DOI: 10.1021/acs.inorgchem.8b02555
Inorg. Chem. XXXX, XXX, XXX−XXX

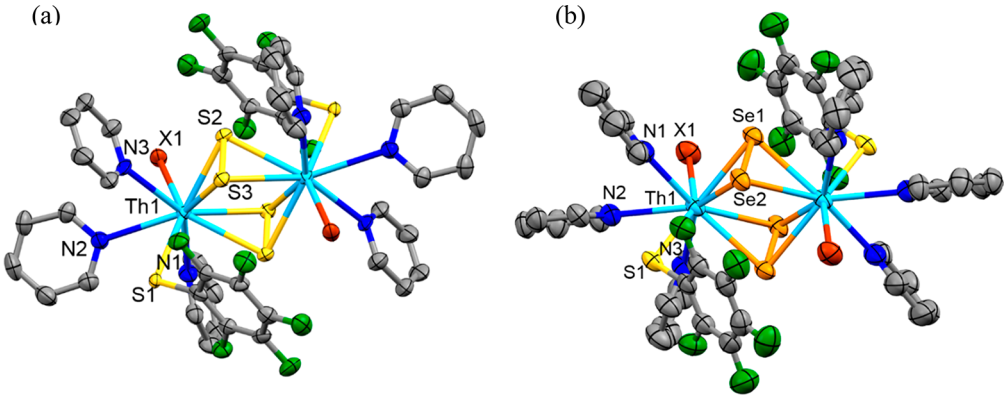

Figure 2. (a) ORTEP diagram of $(py)_6Th_2X_2(SC_6F_5)_2(S_2)_2$, where X = Br (**2**), Cl (**3**). (b) ORTEP diagram of $(py)_6Th_2X_2(SC_6F_5)_2(Se_2)_2$, where X= I (**5**), Br (**6**). Green denotes F, yellow S, orange Se, red halogen(X), light blue Th, dark blue N, and gray C. H atoms are removed for clarity, and ellipsoids are at the 50% probability level. Significant bond length averages are given in Table 1.

Scheme 1. Synthesis of Dichalcogenido-Bridged Thorium Dimers with Terminal Iodides

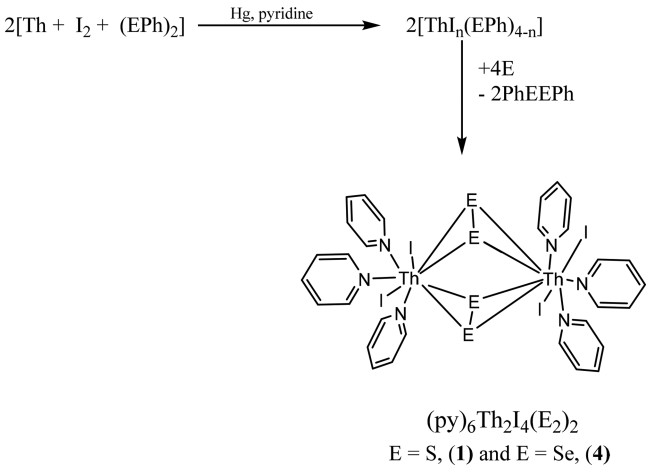

of $(py)_6Th_2I_4(E_2)_2$ (Scheme 1) or $(py)_6Th_2X_2(SC_6F_5)_2(E_2)_2$ (Scheme 2).

A similar redox approach to the synthesis of the disulfide compounds in the presence of chloride ion led to the formation of a product mixture, which includes $(py)_6Th_2Cl_2(SC_6F_5)_2(S_2)_2$ (**3**) and $(py)_4ThCl_4$ (**7**) (Scheme 3). The latter structure has considerable literature precedence.[33]

Similarly, attempts to make a diselenido thorium dimer with terminal fluorothiolate and chloride led to the isolation of a crystalline mixture containing $(py)_4ThCl_4$ and the thorium heterocubane $(py)_8Th_4Se_4(SePh)_4(SC_6F_5)_4$[1b] (Scheme 4).

Compounds **1**−**6** were characterized by spectroscopic methods and low-temperature single-crystal X-ray diffraction. Figure 1 shows an ORTEP diagram of the common molecular structure of **1** and **4**, and Figure 2 shows an ORTEP diagram of the common molecular structure of **2**, **3**, **5**, and **6** from a variety of orientations, with significant bond lengths and angles for **1**−**6** given in Table 1. These are the first examples of thorium compounds with bridging E_2^{2-} ligands.

All six compounds have similar structures containing a central $Th_2(\mu_2\text{-}E_2)_2$ core region, with the primary coordination sphere of each thorium saturated by two additional monodentate anions and three neutral pyridine ligands. The molecular site symmetry of the individual dimer molecules for four of the six compounds is $P2_1/n$, with the exception being the chloride derivative **3** and iodide **5** with fluorothiolates that crystallize in the space group $P\bar{1}$.

Related compounds in the literature are limited. There exists a thorium dimer with two bridging sulfido ligands, $\{[\eta^5\text{-}1,2,4\text{-}(Me_3C)_3C_5H_2]_2Th\}_2(\mu\text{-}S)_2$,[2c] and there are two examples of monometallic thorium compounds with terminally bound η^2-E_2 units, $Cp^*_2Th(DMAP)(S_2)$[3e] and $[Th(Se_2)\{N(SiMe_3)_2\}_3]^-$.[3d] In contrast, there is a more extensive uranium literature, including monometallic species with η^2-E_2 ligands[1e,2e,3a−c,f,g] and bimetallic compounds with one or two bridging E_2 ligands.[2b,e,h,i,3c,4]

Bond geometries for all six compounds summarized in Table 1 are consistent with prior literature, with values reflecting the sizes of the atomic/ionic components. In all six compounds, there are three pyridine molecules bound to thorium(IV), with two of these pyridines (N(1), N(3)) having Th−N bond lengths (2.68−2.72 Å) consistent with the wide range of previously reported Th−N(pyridine) bond lengths: i.e., 2.62−2.72 Å in monomeric $(py)_xTh(ER)_4$,[1a] (x = 3, 4; E = S, Se; R = Ph, C_6F_5), 2.63−2.71 Å in a group of cubane clusters,[1b,s] and 2.730 Å in $(py)_2Th_2(\mu\text{-}OEt_2)_2(OEt_2)_6$.[34] Pyridines opposite to the EE bridges have a slightly longer Th−N(2) bond length (2.73−2.78 Å). The difference in Th−N(1),(3) and Th−N(2) bond lengths within one molecule are about 0.03 Å (compounds **1** and **3**), 0.09 (**2**), 0.01 Å (**4**), 0.07 Å (**5**), and 0.06 Å (**6**).

Thorium−sulfur(thiolate) distances are equally consistent with previous literature values: compare the Th−S(C_6F_5) in nine-coordinate **2** (2.892(2) Å), **3** (average 2.900(9) Å), **5** (average 2.885(4) Å), and **6** (2.884(3) Å) with the Th−S(C_6F_5) bonds in the eight-coordinate cubane clusters $(py)_8Th_4S_4(SPh)_4(SC_6F_5)_4$ (2.900(2) Å)[1b] and $(py)_8Th_4Se_4(SePh)_4(SC_6F_5)_4$ (2.889(2) Å)[1b] and the Th−S bonds in monometallic seven coordinate $(py)_3Th(SC_6F_5)_4$[1a] (2.811−2.825(10) Å).

In all compounds the halide ligands are terminally bound. There are four iodides in **1** (3.174(1), 3.179(1) Å) and **4** (3.197(1), 3.201(1) Å) and two iodides in **5** (average 3.205(1) Å) with nearly identical Th−I bond lengths that are consistent with previously published Th−I distances: i.e., 3.172(1) Å in $(C_5Me_5)_2[^iPrNC(Me)N^iPr\text{-}\kappa^2N,N']ThI$,[35] 3.171(1) Å in $ThI_3[O(CH_2)_4I](THF)_3$,[36] and 3.226(1) Å in $ThI(OCH\,i\text{-}Pr_2)_3(py)_2$.[37] Similarly, complexes **2** and **6** contain terminal bromide ligands with Th−Br bond lengths that are also similar to those in previously reported examples: i.e., 2.895(1) Å in monomeric $(\eta^5\text{-}Cp)_2ThBr_2(THF)$[38] and 2.885(2) Å in heterometallic

DOI: 10.1021/acs.inorgchem.8b02555
Inorg. Chem. XXXX, XXX, XXX−XXX

Scheme 2. Synthesis of Dichalcogenido-Bridged Thorium Dimers with Ancillary Halides and Fluorinated Thiolates

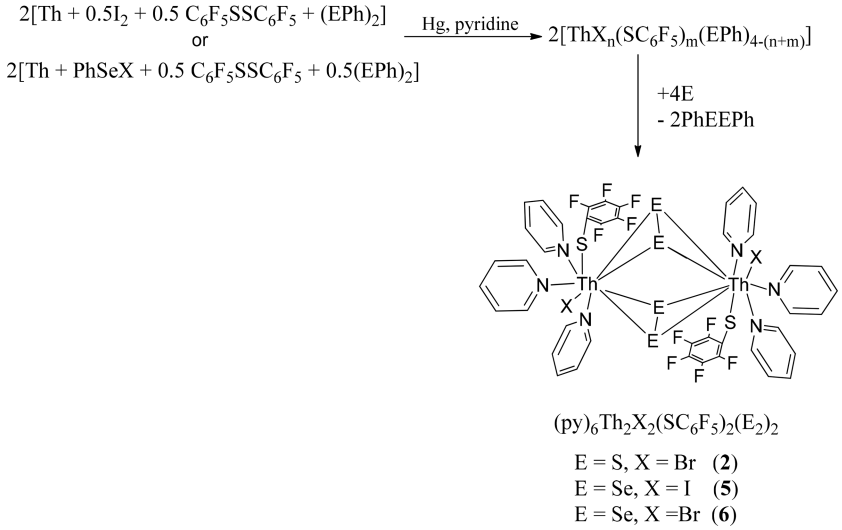

Scheme 3. Synthetic Attempt To Prepare a Disulfide-Bridged Thorium Dimer with Terminally Bound Chloride and Fluorothiolate Ligands

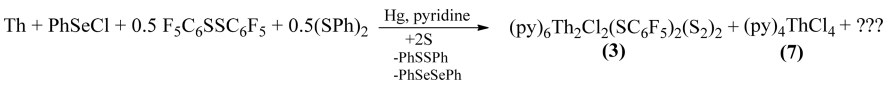

Scheme 4. Synthetic Attempt To Prepare a Diselenido-Bridged Thorium Dimer with Fluorothiolate and Chloride Terminal Ligands

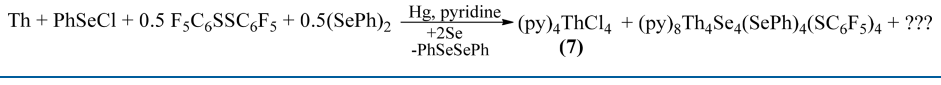

$[(\eta^5\text{-}C_5Me_5)_2Th(Br)N(mesityl)Cu(DMAP))]$.[39] In the single chloride derivative **3**, the Th−Cl bond lengths (average 2.733(8) Å) are again similar to literature values: i.e., 2.755(1) Å in monomeric $Th(TMTAA)Cl_2(THF)_2$[40] and 2.737(1) Å in ThCp*(TMTAA)Cl[40] (TMTAA = tetramethyltetraazaannulene), among others.[14d,39,41]

Disulfido bonds in **1**−**3** are in the range 2.076−2.090(3) Å, consistent with the terminal S_2 unit in the thorium disulfide complex $(\eta^5\text{-}C_5Me_5)_2ThS_2(DMAP)$, which contains a 2.088 Å[3e] sulfur−sulfur bond. Comparable distances[42] have also been noted in uranium,[2e,f,h] lanthanide,[43,44] and transition-metal chemistry.[45] Similarly, dimers **4**−**6** contain Se−Se bonds within a narrow range of bond lengths (2.342−2.350(3) Å) that are almost identical with the 2.397(1) Å for the terminally bound diselenido ligand in $[K(18\text{-crown-}6)][Th(\eta^2\text{-}E_2)(NR_2)_3]$[3d] and fall within the range of expected values for diselenide moieties bound to lanthanides[46] and transition metals.[45h,47]

The molecular conformation of the $[(py)_3ThX(SC_6F_5)E_2]_2$ dimers **2**, **3**, **5**, and **6** can be viewed as having an equatorial plane containing the Th(IV) ions, the centroids of all the py ligands, and the two μ_2-E_2 bridging ligands. In this scheme, the halide and SC_6F_5 ligands extend out of the equatorial plane, such that the X_2S_2 plane is nearly perpendicular to the equatorial plane. This motif makes available a variety of close contacts that are indicative of prevalent intramolecular hydrogen bonding to halogen, chalcogen, and nitrogen acceptor atoms. Further, the py ligands are rotated around their Th−N bonds and this situation brings their α-H atoms into proximity with H-bond acceptors.

Table 2 summarizes close contacts in the compounds **2**, **3**, **5**, and **6**. The van der Waals radii sums (vdW)[48] are also included in Table 2 for comparison. In all of these compounds, intramolecular interactions, which are indicated by distances shorter than vdW radii sums, are found for all α-H on py ligands. For example, in **2**, H(7)···F(5) for py(N1), H(12)···S(1) for py(N2), and H(21)···Br(1) for py(N3) are 0.21, 0.29, and 0.18 Å less than vdW, respectively (Figure 3); in **5**, H(11)···S(1) for py(N1), H(16)···S(1) for py(N2), and H(17)···S(1) for py(N3) are 0.18, 0.25, and 0.27 Å less than vdW, respectively, and in **6**, H(7)···F(1) for py(N1), H(12)···S(1) for py(N2), and H(21)···Br(5) for py(N3) are 0.18, 0.27, and 0.10 Å less than vdW, respectively. Two of these are expected, since F and Br are good electronegative H-bond acceptors. For H···S, the extreme shortness of this contact likely has both the electrostatic basis of the H-bond and the proximity basis of these two atoms more or less confined to a plane perpendicular to the aforementioned equatorial plane of the dimer. As was mentioned earlier, Th(1)−N(2) bonds are much longer (0.09 Å in **2**, 0.07 Å in **5**, and 0.06 Å in **6**) than Th(1)−N(1) and Th(1)−N(3) bonds, and this is consistent with py(N2) having a close contact on only one side of the ligand, versus py(N1) and py(N3) having close contacts on both sides of the py ligand. The situation in **3** is unique. H(12)···S(3) and H(16)···Cl(1) for py (N2) are 0.20 and 0.27 Å less than vdW, respectively. These close contacts from both sides of the py ligand are also consistent with the fact that the Th bond to N(2) is closer than the distance between Th bonds to N(1) and N(3), namely 2.727(8) Å versus 2.720(8) and 2.694(8) Å, in comparison with **2**, **5**, and **6**.

If unit cell packing is viewed along crystallographic *c* axis, the arrangement of neighboring molecules of **6** in the crystallographic *ab* plane is shown in Figure S27. A nearly one

DOI: 10.1021/acs.inorgchem.8b02555
Inorg. Chem. XXXX, XXX, XXX−XXX

Table 1. Ranges of Selected Bond Distances (Å) and Bond Angles (deg) for 1−6

	$(py)_6Th_2I_4S_4{\cdot}2py$ (**1**; $E_2 = S_2$, X = I)	$(py)_6Th_2Br_2(SC_6F_5)_2S_4$ (**2**; $E_2 = S_2$, X = Br)	$(py)_6Th_2Cl_2(SC_6F_5)_2S_4{\cdot}1.5py$ (**3**; $E_2 = S_2$, X = Cl)	$(py)_6Th_2I_4Se_4{\cdot}2py$ (**4**; $E_2 = Se_2$, X = I)	$(py)_6Th_2I_2(SC_6F_5)_2Se_4{\cdot}py$ (**5**; $E_2 = Se_2$, X = I)	$(py)_6Th_2Br_2(SC_6F_5)_2Se_4{\cdot}2py$ (**6**; $E_2 = Se_2$, X = Br)
			Bond Lengths[a]			
Th−N(1),N(3)	2.699(4), 2.702(4)	2.681(7), 2.688(6)	2.669−2.720(8)	2.706(3), 2.710(3)	2.689−2.724(9)	2.684(6), 2.708(7)
Th−N(2)	2.736(4)	2.779(7)	2.727(8), 2.759(8)	2.726(3)	2.755(9), 2.789 (8)	2.775(6)
Th−μ_2-E_2	2.824−2.863(1)	2.852−2.879(2)	2.847−2.875(2)	2.971−3.005 (1)	2.985−3.016(1)	2.994−3.024(1)
Th−η-X	3.174(1), 3.179(1)	2.913(1)	2.738(8), 2.729(8)	3.197(1), 3.201 (1)	3.194(1), 3.216(1)	2.920(2)
Th−η-S(C_6F_5)		2.892(2)	2.894(3), 2.906(9)		2.859(3), 2.911(4)	2.884(2)
E−E	2.076(1)	2.084(3)	2.088(3), 2.090(3)	2.343(1)	2.350(1), 2.345(1)	2.342(1)
S−C		1.733(9)	1.761(16), 1.765(11)		1.782(8), 1.729(9)	1.718(8)
			Bond Angles			
Th−E−Th	88.59−89.00(<1)	90.3−91.12(<1)	89.09−89.95(<1)	86.71−87.04(3)	87.88−88.06(<1)	87.519−87.835(3)
N(1),N(3)−Th−X	87.76−88.34(3)	87.2−87.3(<1)	80.9−86.4(<1)	82.28−86.61(3)	86.0−86.2(<1)	83.89−85.44(<1)
N(2)−Th−X	78.30(8)	77.54(19)	67.8−75.9(<1)	80.38(7)	83.3(<1)	76.68(3)
S−Th−X[b]		144.0−145.12(<1)	148.0−149.0(<1)		146.94−159.0(<1)	147.22(4)
E−Th−X (acute angle)	75.93−77.78(<1)	80.41−83.64(<1)	80.57−84.7(<1)	74.70−74.96(<1)	69.2−72.7(<1)	77.03−80.05(<1)
E−Th−X(obtuse angle)	118.01−120.34(<1)	121.65−125.82(<1)	122.39−126.5(3)	120.49−120.80(3)	115.1−118.6(<1)	121.96−125.39(<1)
Th−S−C		97.4−107.7(<1)	110.3−110.4(<1)		112.2−114.7(<1)	113.0(2)

[a]The ESD values are enclosed in parentheses. Refer to figures for N atom labels. [b]The py ligands have approximately two locations with respect to the Th···Th vector: namely, the axial ligand (N) and the nearly equatorial ligand (N′).

DOI: 10.1021/acs.inorgchem.8b02555
Inorg. Chem. XXXX, XXX, XXX−XXX

Table 2. Summary of H···Y (Y = N, E, or X) Distances (Å) in 2, 3, 5, and 6[a]

$(py)_6Th_2Br_2(SC_6F_5)_2S_4$ (2)[b]	$(py)_6Th_2Cl_2(SC_6F_5)_2S_4$ (3)[c]	$(py)_6Th_2I_2(SC_6F_5)_2Se_4$ (5)	$(py)_6Th_2Br_2(SC_6F_5)_2Se_4$ (6)
	Contacts from py (N1)		
H(7)···S(1) 2.95	**H(7)···S(3) 2.80**	**H(11)···S(1) 2.82**	**H(7)···Se(2) 2.90**
H(7)···F(5) 2.46	**H(7)···F(1) 2.54**	H(11)···F(1) 2.71	**H(7)···F(1) 2.49**
H(11)···Br(1) 2.84	**H(11)···Cl(1) 2.82**	**H(7)···I(1) 3.06**	**H(11)···Br(1) 2.90**
	Contacts from py (N2)		
H(12)···S(1) 2.71	**H(12)···S(3) 2.80**	**H(16)···S(1) 2.75**	**H(12)···S(1) 2.73**
H(12)···N(1) 2.91	H(12)···N(3) 2.86	H(16)···N(1) 2.75	**H(12)···N(1) 2.69**
H(16)···Br(1) 3.01	**H(16)···Cl(1) 2.68**	**H(12)···I(1) 3.09**	**H(16)···Br(1) 3.00**
H(16)···N(3) 2.76	H(16)···N(1) 2.89	**H(12)···N(3) 2.68**	**H(16)···N(3) 2.69**
	Contacts from py (N3)		
H(17)···S(1) 2.78	**H(17)···S(3) 3.09**	**H(17)···S(1) 2.73**	**H(21)···S(1) 2.82**
H(17)···F(1) 2.67	H(17)···F(5) 2.99	**H(17)···F(5) 2.64**	**H(21)···F(5) 2.56**
H(21)···Br(1) 2.87	**H(21)···Cl(1) 2.75**	H(21)···I(1) 3.28	**H(17)···Br(1) 2.95**
H(21)···S(2) 3.27	H(21)···S(2) 3.54	**H(21)···Se(2) 2.96**	H(17)···Se(2) 3.14

[a]Values shorter than the sum of van der Waals radii are given in boldface type. The van der Waals radii sums:[48] 2.75 Å for H···N, 3.00 Å for H···S, 3.10 Å for H···Se, 2.67 Å for H···F, 2.95 Å for H···Cl, 3.05 Å for H···Br, and 3.18 Å for H···I. [b]S(1) is a terminal atom, and S(2) and S(3) are bridging atoms. [c]S(1) and S(2) are bridging atoms, and S(3) is a terminal atom.

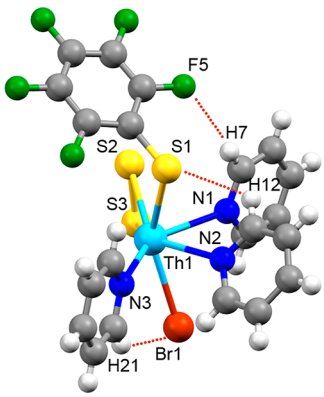

Figure 3. Asymmetric structural unit of compound **2**, with short contacts inside the molecule highlighted.

dimensional (1D) void channel of coordinating py and solvate py molecules along the *c* axis is sandwiched by $Th_2Se_4Br_2(SC_6F_5)_2$ regions. There are also a few intermolecular interactions: i.e., H···F (2.508(1) Å) and H···Se (2.930(1) Å).

DFT Calculations and ^{77}Se NMR Study of Solution Structures. ^{77}Se NMR spectroscopy combined with relativistic DFT calculations and analysis of the measured chemical shifts provides unique insight into the solution structure of diselenido compounds **4**−**6**. Establishing speciation for these molecules is important to fully understand the chemistry of the An−E bond and to realize the ultimate goal of being able to rationally design synthetic approaches to construct increasingly large cluster compounds. Solution and solid-state structures are not necessarily the same, given that strong bases such as pyridine can potentially fragment polymetallic compounds to give products with reduced nuclearity, as illustrated in ionic systems by the reaction of $(THF)_{14}Ln_{10}S_6(Se_2)_6I_6$ with pyridine to give $(py)_6Ln_2(Se_{0.2}S_{0.8})(Se_2)I_2$.[46a]

The experimental ^{77}Se NMR shifts for complexes **4**−**6**, along with those computed for these and other hypothetical thorium dichalcogenide species that could potentially be present in pyridine-d_5 solution, are collected in Table 3. Compounds **4**−**6** show single ^{77}Se NMR resonances at 241, 332, and 309 ppm, respectively (Table 3), all in the range expected for diselenides bridging two Th(IV) ions.

Table 3. Experimental and Computed ^{77}Se NMR Chemical Shifts (in ppm vs Me_2Se) in Selected Thorium Diselenide Complexes[a]

complex	*d*(Th−Se)	DI(Th−Se)	calcd $\delta(^{77}Se)$[b] (ppm)	exptl $\delta(^{77}Se)$[c] (ppm)
$Th_2I_4(\mu_2\text{-}Se_2)_2$ (fully desolvated **4**)	2.948	0.520	469	
$(py)_6Th_2I_4(\mu_2\text{-}Se_2)_2$ (**4**)	2.981	0.456	272	241
$(py)_6Th_2Br_4(\mu_2\text{-}Se_2)_2$	2.994	0.437	267	
$(py)_6Th_2Cl_4(\mu_2\text{-}Se_2)_2$	3.008	0.421	233	
$(py)_6Th_2I_2(SC_6F_5)_2(\mu_2\text{-}Se_2)_2$ (**5**)	2.993	0.443	328	332
$(py)_6Th_2Br_2(SC_6F_5)_2(\mu_2\text{-}Se_2)_2$ (**6**)	2.997	0.436	318	309
$(py)_3ThI_2(\mu_2\text{-}Se_2)$	2.775	0.794	656	
$(py)_4ThI_2(\mu_2\text{-}Se_2)$	2.796	0.738	497	
$(py)_3ThI\ (SC_6F_5)(\mu_2\text{-}Se_2)$	2.788	0.770	678	
$(py)_4ThI\ (SC_6F_5)(\mu_2\text{-}Se_2)$	2.804	0.725	520	
[K(18-crown-6)]$Th(Se_2)(NR_2)_3$	2.914	0.529	273	302[3e]

[a]DFT optimized Th−Se bond lengths, *d*(Th−Se) (in Å), and QTAIM delocalization indices of the Th−Se bonds, DI(Th−Se), are also given. [b]2c-ZORA(SO)/PBE0−40HF/TZ2P results using a COSMO solvation model (cf. Computational Details). Note that the trends in ^{77}Se NMR shifts are dominated by paramagnetic shielding contributions (cf. Table S55 in the Supporting Information). [c]NMR spectra recorded in pyridine-d_5 at room temperature.

Chemical shift calculations were done at the two-component ZORA relativistic level, including spin−orbit (SO) coupling, using the user-customized hybrid PBE0-40HF functional, which was shown to perform very well for a series of monomeric Th selenolates, thorium cubanes $(py)_8Th_4(\mu_3\text{-}E)_4(\mu_2\text{-}E'Ph)_4(\eta\text{-}E'Ph)_4$ (E, E′ = S, Se), and various organoselenides.[1s] The investigated structures were fully optimized at the DFT level (PBE0-D3(BJ)/ECP/def2-TZVP) using quasi-relativistic small-core pseudopotentials for thorium and iodine, along with atom-pairwise corrections for dispersion forces (see Computational Details). First, we note an excellent agreement between X-ray and DFT optimized structures of complexes **1**−**6**, with differences in Th−E, E−E, and Th−X (E = S, Se; X = Br, I, S) bond lengths of less than 0.03 Å (cf. Table 1 and Table S51 in

DOI: 10.1021/acs.inorgchem.8b02555
Inorg. Chem. XXXX, XXX, XXX−XXX

the Supporting Information). Interestingly, one pyridine molecule on each Th atom opposite to the E_2^{2-} bridges (equatorial position with respect to the Th_2X_2 plane) has a notably longer Th−N bond length than the others (by more than 0.07 Å), consistent with the Th−N bond asymmetry observed for axial and equatorial nitrogen atoms in solid-state structures of **1**−**6**, although this inequality is less pronounced in X-ray structures of complexes **1** and **4** (see Table 1 and discussion above). Energy decomposition analysis (EDA) suggests that the longer $Th-N_{py}$ bonds in the equatorial position have an electronic origin resulting from weaker Th−N orbital attractive interactions rather than from steric effects (the latter is comparable with that for axial $Th-N_{py}$ bonds; cf. Table S52 in the Supporting Information). In addition, similar Th−N bond asymmetry for equatorial and axial pyridine ligands is computed for isoelectronic group 4 (Ti, Zr, Hf) congeners of complex **4** (cf. Table S53 in the Supporting Information), showing that this phenomenon is not related to Th(5f) orbitals but to a trans influence of bridging E_2^{2-} moieties, and it also appears in monomeric Th dichalcogenide species (i.e., Th−N bonds in a position trans to the centroid of E_2^{2-} ligands are elongated more than those in the cis position). Adding more pyridine ligands to the first Th coordination sphere in $(py)_6Th_2I_4(\mu_2\text{-}Se_2)_2$ and $(py)_4ThI_4(\mu_2\text{-}Se_2)$ and optimization of these structures at the DFT level results in detachment of these extra py molecules from the metal center, demonstrating the saturated metal coordination environment in isolated dichalcogenide complexes **1**−**6**. In contrast, removal of pyridine ligands leads to somewhat shorter Th−E bonds and elongated E−E contacts (cf. Table S51 in the Supporting Information).

Experimentally observed ^{77}Se NMR shifts for pyridine-d_5 solutions of complexes **4**−**6** match very well with the DFT computed values and are consistent with the dimeric structures being maintained in solution. Not surprisingly, "desolvated" species (with no pyridine ligands attached to thorium) are absent in solution; these hypothetical molecules are computed to be deshielded by about 200 ppm relative to their pyridine-solvated congeners (cf. Table 3), but no ^{77}Se resonance signal in the region 350−1000 ppm was detected. Similarly, ^{77}Se NMR shifts for corresponding monomeric Th species with terminal dichalcogenide ligands are predicted to appear within the range 490−680 ppm (depending on the number of coordinated py molecules; cf. Table 3), thus excluding the dissociation of dimers in solution. In this regard, the dissociation of thorium dimers, $Th_2(\mu_2\text{-}Se_2)$, with two bridging dichalcogenide ligands into monomeric species is computed to be strongly endoergic; specifically, the Gibbs free energies, ΔG°_r, for the dissociation of complex **4** to $(py)_3ThI_2(\mu_2\text{-}Se_2)$ or $(py)_4ThI_2(\mu_2\text{-}Se_2)$ (concomitant with coordination of additional pyridine molecules in the latter case) were calculated to be 30 and 27 kcal/mol, respectively (the PBE0-D3(BJ)/ECP/def2-TZVP result; cf. Table S54 in the Supporting Information). We note further that although ^{77}Se NMR shifts observed herein for dimeric structures resemble the value measured for a thorium complex with a "terminal" Se_2^{2-} ligand, $[K(18\text{-crown-}6)][Th(Se_2)(NR_2)_3]$ ($\delta(^{77}Se)$ 302 ppm in pyridine-d_5),[3d] this coincidence can be attributed to the anionic nature of the latter, which is reflected in its elongated Th−Se bonds and reduced Th−Se covalency in comparison to neutral mononuclear Th diselenides (cf. Table 3). Replacing iodide ligands with lighter analogues (Br^-, Cl^-) leads to slightly longer Th−Se distances that are also reflected in small but notable upfield ^{77}Se shifts, as are also evident from experimental data for complexes **5** and **6**. This can be rationalized by stronger π-donating abilities within the row $I^- < Br^- < Cl^-$, which in turn weakens the Th−Se bond covalency in mixed Th chalcogenide−halide complexes on going up the halogen group, and might be the reason for the lower stability of dimeric Th_2E_4 species with terminal Cl^- ligands.

UV−Vis Absorption Spectra. In contrast to colorless compounds **1**−**3**, complexes **4**−**6** are yellow to yellow-orange in the solid-state as well as in pyridine solution. The UV−vis absorption spectrum of compound **4** is given in Figure S22 of the Supporting Information, showing the strongest absorption band at about 310 nm, followed by an intense absorption without a distinct maximum reaching a plateau at about 440 nm and a steadily decreasing absorption within the wavelength range of 400−500 nm. To understand the nature of the electronic transitions, we performed time-dependent DFT calculations of excitation energies (see Table S56 and Figure 28 in the Supporting Information) for isostructural compounds **1** (colorless $(py)_6Th_2I_4(\mu_2\text{-}S_2)_2$) and **4** (yellow $(py)_6Th_2I_4(\mu_2\text{-}Se_2)_2$). The profile of the TD-DFT simulated absorption spectrum of **4** agrees well with experiment (cf. Figures S22 and S28 in the Supporting Information) and thus allows assignment of the most intense bands (cf. Table S56 and Figure S29 in the Supporting Information). Hence, it is clear that the strongest peak in the UV region (∼310 nm) can be primarily assigned to excitations from nonbonding lone pairs on the bridging selenium atoms (HOMO-1) to predominantly metal-centered MOs with a large Th(5f) contribution (LUMO +13, LUMO+17), followed by less intense excitations from the Se lone pairs to pyridine ligands (∼350 nm, HOMO-1 → LUMO+7 transition). The absorption in the visible (violet) region (370−410 nm) is primarily related to transitions from the Th−Se bonding MOs (HOMO, HOMO-2) and nonbonding Se lone pairs (HOMO-1) to selenium antibonding MOs (LUMO+3). Since the latter excitation energies corresponding to the $n(E_2^{2-}) \rightarrow \pi^*(E_2^{2-})$ transition are shifted hypsochromically in disulfide complexes, these appear as colorless. We note in passing that the yellow color is also observed for some lanthanide di- and triselenide complexes[46a,49] that can be similarly related to $n(Se_2^{2-}) \rightarrow \pi^*(Se_2^{2-})$ transitions and that the behavior of related telluride compounds[50] is also consistent with this interpretation.

Thermolysis. Thermolysis[1a,51] of carefully designed molecular precursors is potentially useful as a low-temperature synthesis approach to metastable solid-state materials, with compounds **1** and **4** presenting an opportunity to explore the low-temperature preparation of ternary solid-state materials. Of the two, the I/SeSe combination found in **4** was the most promising candidate to form a ternary phase at elevated temperatures because of the relative electronegativity of I and Se. Compounds with fluorinated thiolate ligands are complicated by the tendency of Th to abstract F and form ThF_4, and the more electronegative sulfur in **1** favors the formation of ThS_2 rather than ThI_2S or $ThI_2(S_2)$. Thermolysis of **4** was performed under the same conditions as previously reported for[1a] $(py)_3Th(SePh)_4$. The PXRD analysis revealed that $ThSe_2$[52] is the only solid-state product, with no evidence for the formation of any ternary ThISe phases. The surface morphology of the resulting powder of the thermal residual is shown in Figure 4 by SEM, and this $ThSe_2$ stoichiometry was also confirmed by EDS (Figure S25), with trace (<3%) iodide present. GC/MS analysis of the volatile products identified both pyridine and elemental iodine (Scheme 5).

DOI: 10.1021/acs.inorgchem.8b02555
Inorg. Chem. XXXX, XXX, XXX−XXX

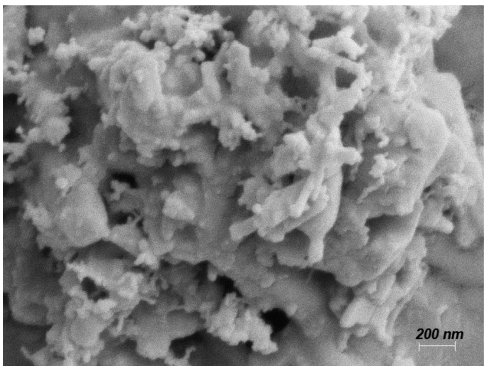

Figure 4. SEM images of $ThSe_2$ (in 200 nm scale) obtained from the thermolysis of compound **4**.

Scheme 5. Thermal Decomposition of $(py)_6Th_2I_4(Se_2)_2$.

$$(py)_6Th_2I_4(Se_2)_2 \xrightarrow{850^{o}C} 2\ ThSe_2 + 2\ I_2 + 6\ py$$

CONCLUSIONS

Remarkably simple chalcogen-rich Th dimers containing E_2^{2-} (E = S, Se) bridging ligands can be prepared with a range of sterically undemanding ancillary ligands, including both halogens and fluorinated thiolates. These compounds are fundamentally important starting materials for our ultimate goal of rationally approaching increasingly large actinide and heterometallic actinide/transition-metal cluster compounds. The solution ^{77}Se NMR spectra are consistent with the dimeric structure being maintained in pyridine solution. Thermolysis of the dimer containing both I^- and Se_2^{2-} ligands resulted in reductive cleavage of the Se−Se bond, oxidative elimination of I_2, and formation of solid-state $ThSe_2$.

ASSOCIATED CONTENT

Supporting Information

The Supporting Information is available free of charge on the ACS Publications website at DOI: 10.1021/acs.inorgchem.8b02555.

Calculated and observed PXRD profiles for **1**−**7**, crystallographic data for **1**−**7**, IR and NMR spectra, and calculated ^{77}Se NMR shieldings and their decomposition into individual contributions (PDF)

Cartesian coordinates of the DFT-optimized structures (XYZ)

Accession Codes

CCDC 1853617−1853623 contain the supplementary crystallographic data for this paper. These data can be obtained free of charge via www.ccdc.cam.ac.uk/data_request/cif, or by emailing data_request@ccdc.cam.ac.uk, or by contacting The Cambridge Crystallographic Data Centre, 12 Union Road, Cambridge CB2 1EZ, UK; fax: +44 1223 336033.

AUTHOR INFORMATION

Corresponding Author

*E-mail for J.G.B.: bren@rci.rutgers.edu.

*E-mail for P.H.: peter.hrobarik@uniba.sk.

ORCID

Peter Hrobárik: 0000-0002-6444-8555

John G. Brennan: 0000-0002-3994-221X

Notes

The authors declare no competing financial interest.

ACKNOWLEDGMENTS

This material is based upon work supported by the National Science Foundation under CHE-1464887. The computational work has been supported by the Ministry of Education, Science, Research and Sport of the Slovak Republic and by the Slovak Research and Development Agency under contracts 1/0712/18 (VEGA) and APVV-17-0324, respectively. P.H. also acknowledges funding from the European Union's Horizon 2020 research and innovation program under the Marie Skłodowska-Curie Grant No. 752285.

REFERENCES

(1) (a) Rehe, D.; Kornienko, A. Y.; Emge, T. J.; Brennan, J. G. Thorium Compounds with Bonds to Sulfur or Selenium: Synthesis, Structure, and Thermolysis. *Inorg. Chem.* **2016**, *55*, 6961−6967. (b) Stuber, M. A.; Kornienko, A. Y.; Emge, T. J.; Brennan, J. G. Tetrametallic Thorium Compounds with Th_4E_4 (E = S, Se) Cubane Cores. *Inorg. Chem.* **2017**, *56*, 10247−10256. (c) Arliguie, T.; Thuery, P.; Le Floch, P.; Mezailles, N.; Ephritikhine, M. A homoleptic SPS-based complex and a double-cubane-type sulfur cluster of an actinide element. *Polyhedron* **2009**, *28*, 1578−1582. (d) Gaunt, A. J.; Scott, B. L.; Neu, M. P. U(IV) chalcogenolates synthesized via oxidation of uranium metal by dichalcogenides. *Inorg. Chem.* **2006**, *45*, 7401−7407. (e) Siladke, N. A.; Ziller, J. W.; Evans, W. J. Insertion, Isomerization, and Cascade Reactivity of the Tethered Silylalkyl Uranium Metallocene $(\eta^5\text{-}C_5Me_4SiMe_2CH_2\text{-}\kappa C)_2U$. *J. Am. Chem. Soc.* **2011**, *133*, 3507−3516. (f) Tang, Y. X.; Deng, J. Y.; Li, W. L.; Malyi, O. I.; Zhang, Y. Y.; Zhou, X. R.; Pan, S. W.; Wei, J. Q.; Cai, Y. R.; Chen, Z.; Chen, X. D. Water-Soluble Sericin Protein Enabling Stable Solid-Electrolyte Interphase for Fast Charging High Voltage Battery Electrode. *Adv. Mater.* **2017**, *29*, 1701828. (g) Smiles, D. E.; Wu, G.; Hayton, T. W. Synthesis, Electrochemistry, and Reactivity of the Actinide Trisulfides $[K(18\text{-crown-}6)][An(\eta^3\text{-}S_3)(NR_2)_3]$ (An = U, Th; R = $SiMe_3$). *Inorg. Chem.* **2016**, *55*, 9150−9153. (h) Franke, S. M.; Rosenzweig, M. W.; Heinemann, F. W.; Meyer, K. Reactivity of uranium(III) with H_2E (E = S, Se, Te): synthesis of a series of mononuclear and dinuclear uranium(IV) hydrochalcogenido complexes. *Chem. Sci.* **2015**, *6*, 275−282. (i) Gaunt, A. J.; Scott, B. L.; Neu, M. P. A molecular actinide-tellurium bond and comparison of bonding in $[M^{III}\{N(TeP\mathit{i}Pr_2)_2\}_3]$ (M = U, La). *Angew. Chem., Int. Ed.* **2006**, *45*, 1638−1641. (j) Jones, R. G.; Karmas, G.; Martin, G. A., Jr.; Gilman, H. Organic compounds of Uranium. II. Uranium (IV) amides, alkoxides and mercaptides. *J. Am. Chem. Soc.* **1956**, *78*, 4285−4286. (k) Zhou, E.; Ren, W.; Hou, G.; Zi, G.; Fang, D.; Walter, M. D. Small Molecule Activation Mediated by a Thorium Terminal Imido Metallocene. *Organometallics* **2015**, *34*, 3637−3647. (l) Evans, W. J.; Takase, M. K.; Ziller, J. W.; DiPasquale, A. G.; Rheingold, A. L. Reductive Reactivity of the Tetravalent Uranium Complex $[\eta^5\text{-}C_5Me_5)(\eta^8\text{-}C_8H_8)U]_2(\mu\text{-}\eta^3\text{:}\eta^3\text{-}C_8H_8)$. *Organometallics* **2009**, *28*, 236−243. (m) Ren, W.; Zi, G.; Walter, M. D. Synthesis, Structure, and Reactivity of a Thorium Metallocene Containing a 2,2 '-Bipyridyl Ligand. *Organometallics* **2012**, *31*, 672−679. (n) Leverd, P. C.; Ephritikhine, M.; Lance, M.; Vigner, J.; Nierlich, M. Triscyclopentadienyl uranium thiolates and selenolates. *J. Organomet. Chem.* **1996**, *507*, 229−237. (o) Evans, W. J.; Miller, K. A.; Ziller, J. W.; DiPasquale, A. G.; Heroux, K. J.; Rheingold, A. L. Formation of $(C_5Me_5)_2U(EPh)Me$, $(C_5Me_5)_2U(EPh)_2$, and $(C_5Me_5)_2U(\eta^2\text{-}TeC_6H_4)$ from $(C_5Me_5)_2UMe_2$ and PhEEPh (E = S, Se, Te). *Organometallics* **2007**, *26*, 4287−4293. (p) Thomson, R. K.; Graves, C. R.; Scott, B. L.; Kiplinger, J. L. Synthesis and Molecular Structure of $(C_5Me_5)_2U(O^tBu)(SePh)$: A Mixed-Ligand Alkoxide-Selenide Uranium(IV) Metallocene Complex Resulting from *tert*-Butoxy-Trimethylsilane Elimination. *J. Chem. Crystallogr.* **2011**, *41*, 1241−1244. (q) Domingos, A.; Dematos, A. P.; Santos, I. Synthesis and Characterization of the Uranium Alkylthiolate Complex $U(Spr^i)_2(HBPz_3)_2$. *Polyhedron* **1992**, *11*, 1601−1606. (r) Matson, E. M.; Breshears, A. T.; Kiernicki, J. J.; Newell, B. S.; Fanwick, P. E.;

DOI: 10.1021/acs.inorgchem.8b02555
Inorg. Chem. XXXX, XXX, XXX−XXX

Shores, M. P.; Walensky, J. R.; Bartt, S. C. Trivalent Uranium Phenylchalcogenide Complexes: Exploring the Bonding and Reactivity with CS_2 in the Tp^*_2UEPh Series (E = O, S, Se, Te). *Inorg. Chem.* **2014**, *53*, 12977−12985. (s) Ringgold, M.; Rehe, D.; Hrobarik, P.; Kornienko, A. Y.; Emge, T. J.; Brennan, J. G. Thorium Cubanes-Synthesis, Solid-State and Solution Structures, Thermolysis, and Chalcogen Exchange Reactions. *Inorg. Chem.* **2018**, *57*, 7129−7141. (t) Ringgold, M.; Wu, W.; Stuber, M.; Kornienko, A. Y.; Emge, T. J.; Brennan, J. G. Monomeric thorium chalcogenolates with bipyridine and terpyridine ligands. *Dalton Trans* **2018**, *47*, 14652−14661.

(2) (a) Benaud, O.; Berthet, J. C.; Thuery, P.; Ephritikhine, M. CCDC 958676. *CSD Commun.*. **2013**. (b) Lam, O. P.; Heinemann, F. W.; Meyer, K. Activation of elemental S, Se and Te with uranium(III): bridging U-E-U (E = S, Se) and diamond-core complexes U-$(E)_2$-U (E = O, S, Se, Te). *Chem. Sci.* **2011**, *2*, 1538−1547. (c) Ren, W.; Zi, G.; Fang, D.; Walter, M. D. Thorium Oxo and Sulfido Metallocenes: Synthesis, Structure, Reactivity, and Computational Studies. *J. Am. Chem. Soc.* **2011**, *133*, 13183−13196. (d) Chatelain, L.; White, S.; Scopelliti, R.; Mazzanti, M. Isolation of a Star-Shaped Uranium(V/VI) Cluster from the Anaerobic Photochemical Reduction of Uranyl(VI). *Angew. Chem., Int. Ed.* **2016**, *55*, 14325−14327. (e) Camp, C.; Antunes, M. A.; Garcia, G.; Ciofini, I.; Santos, I. C.; Pecaut, J.; Almeida, M.; Marcalo, J.; Mazzanti, M. Two-electron versus one-electron reduction of chalcogens by uranium(III): synthesis of a terminal U(V) persulfide complex. *Chem. Sci.* **2014**, *5*, 841−846. (f) Gardner, B. M.; King, D. M.; Tuna, F.; Wooles, A. J.; Chilton, N. F.; Liddle, S. T. Assessing crystal field and magnetic interactions in diuranium-μ-chalcogenide triamidoamine complexes with U^{IV}-E-U^{IV} cores (E = S, Se, Te): implications for determining the presence or absence of actinide-actinide magnetic exchange. *Chem. Sci.* **2017**, *8*, 6207−6217. (g) Arnold, P. L.; Stevens, C. J.; Bell, N. L.; Lord, R. M.; Goldberg, J. M.; Nichol, G. S.; Love, J. B. Multi-electron reduction of sulfur and carbon disulfide using binuclear uranium(III) borohydride complexes. *Chem. Sci.* **2017**, *8*, 3609−3617. (h) Brown, J. L.; Wu, G.; Hayton, T. W. Chalcogen Atom Transfer to Uranium(III): Synthesis and Characterization of $[(R_2N)_3U]_2(\mu\text{-E})$ and $[(R_2N)_3U]_2(\mu\text{-}\eta^2\text{:}\eta^2\text{-}S_2)$ (R = $SiMe_3$; E = S, Se, Te). *Organometallics* **2013**, *32*, 1193−1198. (i) Franke, S. M.; Heinemann, F. W.; Meyer, K. Reactivity of uranium(IV) bridged chalcogenido complexes U^{IV}-E-U^{IV} (E = S. Se) with elemental sulfur and selenium: synthesis of polychalcogenido-bridged uranium complexes. *Chem. Sci.* **2014**, *5*, 942−950. (j) Avens, L. R.; Barnhart, D. M.; Burns, C. J.; Mckee, S. D.; Smith, W. H. Oxidation Chemistry of a Uranium(III) Aryloxide. *Inorg. Chem.* **1994**, *33*, 4245−4254. (k) Clark, D. L.; Gordon, J. C.; Huffman, J. G.; Watkin, J. G.; Zwick, B. D. Preparation of Mono-Pentamethylcyclopentadienyl Uranium(IV) Sulfido Clusters through Oxidation of $(\eta\text{-}C_5Me_5)_3U_3(\mu_3\text{-S})(\mu_2\text{-I})_3I_3$. *New J. Chem.* **1995**, *19*, 495−502. (l) Evans, W. J.; Montalvo, E.; Ziller, J. W.; DiPasquale, A. G.; Rheingold, A. L. Uranium Metallocene Complexes of the 1,3,4,6,7,8-Hexahydro-2*H*-pyrimido[1,2-a]pyrimidinato Ligand, $(hpp)^-$. *Inorg. Chem.* **2010**, *49*, 222−228. (m) Thevenin, T. L.; Wilmarth, W. R.; Peterson, J. R.; Haire, R. G. New Ternary Trans-Uranium Compounds: Chalcogenide Halides. *Mater. Res. Bull.* **1988**, *23*, 851−855. (n) Groom, C. R.; Bruno, I. J.; Lightfoot, M. P.; Ward, S. C. The Cambridge Structural Database. *Acta Crystallogr., Sect. B: Struct. Sci., Cryst. Eng. Mater.* **2016**, *72*, 171−179.

(3) (a) Perry, D. L.; Zalkin, A.; Ruben, H.; Templeton, D. H. Synthesis, Characterization, and Structure of a Uranyl Complex with a Disulfide Ligand, Bis(di-n-Propylammonium) Disulfidobis(di-n-Propylthiocarbamato)dioxouranate(VI). *Inorg. Chem.* **1982**, *21*, 237−240. (b) Smiles, D. E.; Wu, G.; Hayton, T. W. Reversible Chalcogen-Atom Transfer to a Terminal Uranium Sulfide. *Inorg. Chem.* **2014**, *53*, 12683−12685. (c) Smiles, D. E.; Wu, G.; Hayton, T. W. Reactivity of $[U(CH_2SiMe_2NSiMe_3)(NR_2)_2]$ (R = $SiMe_3$) with elemental chalcogens: towards a better understanding of chalcogen atom transfer in the actinides. *New J. Chem.* **2015**, *39*, 7563−7566. (d) Smiles, D. E.; Wu, G.; Hrobarik, P.; Hayton, T. W. Use of ^{77}Se and ^{125}Te NMR Spectroscopy to Probe Covalency of the Actinide-Chalcogen Bonding in $[Th(E_n)\{N(SiMe_3)_2\}_3]^-$ (E = Se, Te; n = 1, 2) and Their Oxo-Uranium(VI) Congeners. *J. Am. Chem. Soc.* **2016**, *138*, 814−825. (e) Yang, P.; Zhou, E.; Fang, B.; Hou, G.; Zi, G.; Walter, M. D. Preparation of $(\eta^5\text{-}C_5Me_5)_2Th(bipy)$ and Its Reactivity toward Small Molecules. *Organometallics* **2016**, *35*, 2129−2139. (f) Matson, E. M.; Goshert, M. D.; Kiernicki, J. J.; Newell, B. S.; Fanwick, P. E.; Shores, M. P.; Walensky, J. R.; Bart, S. C. Synthesis of Terminal Uranium(IV) Disulfido and Diselenido Compounds by Activation of Elemental Sulfur and Selenium. *Chem. - Eur. J.* **2013**, *19*, 16176−16180. (g) Grant, D. J.; Weng, Z. H.; Jouffret, L. J.; Burns, P. C.; Gagliardi, L. Synthesis of a Uranyl Persulfide Complex and Quantum Chemical Studies of Formation and Topologies of Hypothetical Uranyl Persulfide Cage Clusters. *Inorg. Chem.* **2012**, *51*, 7801−7809.

(4) Andrez, J.; Pecaut, J.; Scopelliti, R.; Kefalidis, C. E.; Maron, L.; Rosenzweig, M. W.; Meyer, K.; Mazzanti, M. Synthesis and reactivity of a terminal uranium(IV) sulfide supported by siloxide ligands. *Chem. Sci.* **2016**, *7*, 5846−5856.

(5) Spencer, L. P.; Yang, P.; Scott, B. L.; Batista, E. R.; Boncella, J. M. Oxidative Addition to U(V)-U(V) Dimers: Facile Routes to Uranium(VI) Bis(imido) Complexes. *Inorg. Chem.* **2009**, *48*, 11615−11623.

(6) Wrobleski, D. A.; Cromer, D. T.; Ortiz, J. V.; Rauchfuss, T. B.; Ryan, R. R.; Sattelberger, A. P. Preparation and Characterization of the First Organoactinide Polysulfide $(\eta^5\text{-}C_5Me_5)_2ThS5$. A Unique Example of the Twist-Boat Conformation of the MS_5 Ring. *J. Am. Chem. Soc.* **1986**, *108*, 174−175.

(7) (a) Smiles, D. E.; Wu, G.; Kaltsoyannis, N.; Hayton, T. W. Thorium-ligand multiple bonds via reductive deprotection of a trityl group. *Chem. Sci.* **2015**, *6*, 3891−3899. (b) Clark, D. L.; Miller, M. M.; Watkin, J. G. Synthesis, Characterization, and X-Ray Structure of the Uranium Thiolate Complex $U(S\text{-}2,6\text{-}Me_2C_6H_3)[N(SiMe_3)_2]_3$. *Inorg. Chem.* **1993**, *32*, 772−774. (c) Roger, M.; Barros, N.; Arliguie, T.; Thuery, P.; Maron, L.; Ephritikhine, M. $U(SMes^*)_n$, (n = 3, 4) and $Ln(SMes^*)_3$ (Ln = La, Ce, Pr, Nd): Lanthanide(III)/actinide-(III) differentiation in agostic interactions and an unprecedented η^3 Ligation mode of the arylthiolate ligand, from X-ray diffraction and DFT analysis. *J. Am. Chem. Soc.* **2006**, *128*, 8790−8802. (d) Brown, J. L.; Fortier, S.; Lewis, R. A.; Wu, G.; Hayton, T. W. A Complete Family of Terminal Uranium Chalcogenides, $[U(E)(N\{SiMe_3\}_2)_3]^-$ (E = O, S, Se, Te). *J. Am. Chem. Soc.* **2012**, *134*, 15468−15475.

(8) (a) Zhang, L.; Fang, B.; Hou, G.; Ai, L.; Ding, W.; Walter, M. D.; Zi, G. Intrinsic reactivity of a uranium metallacyclopropene toward unsaturated organic molecules. *Dalton Trans* **2016**, *45*, 16441−16452. (b) Montalvo, E.; Miller, K. A.; Ziller, J. W.; Evans, W. J. Reactivity of Tuck-in and Tuck-over Uranium Metallocene Complexes. *Organometallics* **2010**, *29*, 4159−4170. (c) Barnea, E.; Andrea, T.; Kapon, M.; Eisen, M. S. Formation of inclusion organoactinide complexes with boron-containing macrocycles. *J. Am. Chem. Soc.* **2004**, *126*, 5066−5067. (d) Zhang, L.; Hou, G.; Zi, G.; Ding, W.; Walter, M. D. Preparation of a uranium metallacyclocumulene and its reactivity towards unsaturated organic molecules. *Dalton Trans* **2017**, *46*, 3716−3728. (e) Ren, W.; Song, H.; Zi, G.; Walter, M. D. A bipyridyl thorium metallocene: synthesis, structure and reactivity. *Dalton Trans* **2012**, *41*, 5965−5973. (f) Graves, C. R.; Scott, B. L.; Morris, D. E.; Kiplinger, J. L. Selenate and tellurate complexes of pentavalent uranium. *Chem. Commun.* **2009**, 776−778. (g) Zalkin, A.; Brennan, J. G. A Trivalent-Uranium Thioether Coordination Compound. *Acta Crystallogr., Sect. C: Cryst. Struct. Commun.* **1985**, *41*, 1295−1297. (h) Brennan, J. G.; Andersen, R. A.; Zalkin, A. Chemistry of Trivalent Uranium Metallocenes: Electron-Transfer Reactions with Carbon Disulfide. Formation of $[(RC_5H_4)_3U]_2[\mu\text{-}\eta^1, \eta^2\text{-}CS_2]$. *Inorg. Chem.* **1986**, *25*, 1756−1760. (i) Siladke, N. A.; LeDuc, J.; Ziller, J. W.; Evans, W. J. Synthesis and Insertion Chemistry of Mixed Tether Uranium Metallocene Complexes. *Chem. - Eur. J.* **2012**, *18*, 14820−14827. (j) Fang, B.; Ren, W.; Hou, G.; Zi, G. F.; Fang, D.; Maron, L.; Walter, M. D. An Actinide Metallacyclopropene Complex: Synthesis, Structure, Reactivity, and Computational Studies. *J. Am. Chem. Soc.* **2014**, *136*, 17249−17261. (k) Evans, W. J.; Walensky, J. R.; Ziller, J. W. Reaction Chemistry of the U^{3+} Metallocene Amidinate $(C_5Me_5)_2[^iPrNC(Me)N^iPr]U$ Including the Isolation of a Uranium

DOI: 10.1021/acs.inorgchem.8b02555
Inorg. Chem. XXXX, XXX, XXX−XXX

Complex of a Monodentate Acetate. *Inorg. Chem.* **2010**, *49*, 1743−1749. (l) Ventelon, L.; Lescop, C.; Arliguie, T.; Leverd, P. C.; Lance, M.; Nierlich, M.; Ephritikhine, M. Synthesis and X-ray crystal structure of [Na(18-crown-6)][U(Cp*)$_2$(SBu^t)(S)], the first f-element compound containing a metal-sulfur double bond. *Chem. Commun.* **1999**, 659−660. (m) Lin, Z. R.; Brock, C. P.; Marks, T. J. Synthesis, Structural Characterization, and Properties of the Organothorium Alkylthiolate Complex [(CH$_3$)$_5$C$_5$]$_2$Th(SCH$_2$CH$_2$CH$_3$)$_2$. *Inorg. Chim. Acta* **1988**, *141*, 145−149. (n) Arliguie, T.; Blug, M.; Le Floch, P.; Mezailles, N.; Thuery, P.; Ephritikhine, M. Organouranium complexes with phosphinine-based SPS pincer ligands. Variations with the substituent at the phosphorus atom. *Organometallics* **2008**, *27*, 4158−4165. (o) Tourneux, J. C.; Berthet, J. C.; Thuery, P.; Mezailles, N.; Le Floch, P.; Ephritikhine, M. Easy access to uranium nucleophilic carbene complexes. *Dalton Trans* **2010**, *39*, 2494−2496. (p) Fang, B.; Zhang, L.; Hou, G.; Zi, G.; Fang, D.-C.; Walter, M. D. Experimental and Computational Studies on an Actinide Metallacyclocumulene Complex. *Organometallics* **2015**, *34*, 5669−5681. (q) Cao, Y.; Kobayashi, N.; Zhang, Y. W.; Ohnuma, S.; Masumoto, H. Enhanced spin-dependent charge transport of Co-(Al-fluoride) granular nanocomposite by co-separate sputtering. *J. Appl. Phys.* **2017**, *122*, 133903. (r) Kiernicki, J. J.; Staun, S. L.; Zeller, M.; Bart, S. C. A Uranium(IV) Triamide Species with Bronsted Basic Ligand Character: Metal Ligand Cooperativity in the f Block. *Organometallics* **2017**, *36*, 665−672. (s) Formanuik, A.; Ortu, F.; Inman, C. J.; Kerridge, A.; Castro, L.; Maron, L.; Mills, D. P. Concomitant Carboxylate and Oxalate Formation From the Activation of CO$_2$ by a Thorium(III) Complex. *Chem. - Eur. J.* **2016**, *22*, 17976−17979. (t) Tourneux, J. C.; Berthet, J. C.; Cantat, T.; Thuery, P.; Mezailles, N.; Le Floch, P.; Ephritikhine, M. Uranium(IV) Nucleophilic Carbene Complexes. *Organometallics* **2011**, *30*, 2957−2971. (u) Roger, M.; Belkhiri, L.; Thuery, P.; Arliguie, T.; Fourmigue, M.; Boucekkine, A.; Ephritikhine, M. Lanthanide(III)/actinide(III) differentiation in mixed cyclopentadienyl/dithiolene compounds from X-ray diffraction and density functional theory analysis. *Organometallics* **2005**, *24*, 4940−4952. (v) Arliguie, T.; Lescop, C.; Ventelon, L.; Leverd, P. C.; Thuery, P.; Nierlich, M.; Ephritikhine, M. C-H and C-S bond cleavage in uranium(III) thiolato complexes. *Organometallics* **2001**, *20*, 3698−3703. (w) Evans, W. J.; Miller, K. A.; Kozimor, S. A.; Ziller, J. W.; DiPasquale, A. G.; Rheingold, A. L. Actinide hydride complexes as multielectron reductants: Analogous reduction chemistry from [(C$_5$Me$_5$)$_2$UH]$_2$, [(C$_5$Me$_5$)$_2$UH$_2$]$_2$, and [(C$_5$Me$_5$)$_2$ThH$_2$]$_2$. *Organometallics* **2007**, *26*, 3568−3576. (x) Ren, W.; Lukens, W. W.; Zi, G.; Maron, L.; Walter, M. D. Is the bipyridyl thorium metallocene a low-valent thorium complex? A combined experimental and computational study. *Chem. Sci.* **2013**, *4*, 1168−1174. (y) Lescop, C.; Arliguie, T.; Lance, M.; Nierlich, M.; Ephritikhine, M. Bispentamethylcyclopentadienyl uranium(IV) thiolate compounds. Synthesis and reactions with CO$_2$ and CS$_2$. *J. Organomet. Chem.* **1999**, *580*, 137−144. (z) Mehdoui, T.; Berthet, J. C.; Thuery, P.; Ephritikhine, M. CCDC 958639. *CSD Commun.* **2014**. (aa) Evans, W. J.; Miller, K. A.; Hillman, W. R.; Ziller, J. W. Two-electron reductive reactivity of trivalent uranium tetraphenylborate complexes of (C$_5$Me$_5$)$^{1-}$ and (C$_5$Me$_4$H)$^{1-}$. *J. Organomet. Chem.* **2007**, *692*, 3649−3654. (ab) Roger, M.; Belkhiri, L.; Arliguie, T.; Thuery, P.; Boucekkine, A.; Ephritikhine, M. Uranium and lanthanide complexes with the 2-mercapto benzothiazolate ligand: Evidence for a specific covalent binding site in the differentiation of isostructural lanthanide(III) and actinide(III) compounds. *Organometallics* **2008**, *27*, 33−42. (ac) Graves, C. R.; Scott, B. L.; Morris, D. E.; Kiplinger, J. L. Facile access to pentavalent uranium organometallics: One-electron oxidation of Uranium(IV) imido complexes with copper(I) salts. *J. Am. Chem. Soc.* **2007**, *129*, 11914−11915. (ad) Kiernicki, J. J.; Fanwick, P. E.; Bart, S. C. Utility of a redox-active pyridine(diimine) chelate in facilitating two electron oxidative addition chemistry at uranium. *Chem. Commun.* **2014**, *50*, 8189−8192. (ae) Ephritikhine, M. Recent Advances in Organo-actinide Chemistry As Exemplified by Cyclopentadienyl Compounds. *Organometallics* **2013**, *32*, 2464−2488. (af) Zi, G. Recent developments in actinide metallacycles. *Chem. Commun.* **2018**, *54*, 7412−7430.

(9) Campello, M. P. C.; Domingos, A.; Galvao, A.; de Matos, A. P.; Santos, I. Derivative chemistry of [UCl$_2${B(pz)$_4$}$_2$]: stability of complexes containing the fragments [U{B(pz)$_4$}$_2$] and [U{HB(pz)$_3$}$_2$]. *J. Organomet. Chem.* **1999**, *579*, 5−17.

(10) (a) Smiles, D. E.; Wu, G.; Hayton, T. W. Synthesis of Uranium-Ligand Multiple Bonds by Cleavage of a Trityl Protecting Group. *J. Am. Chem. Soc.* **2014**, *136*, 96−99. (b) Brown, J. L.; Fortier, S.; Wu, G.; Kaltsoyannis, N.; Hayton, T. W. Synthesis and Spectroscopic and Computational Characterization of the Chalcogenido-Substituted Analogues of the Uranyl Ion, [OUE]$^{2+}$ (E = S, Se). *J. Am. Chem. Soc.* **2013**, *135*, 5352−5355.

(11) (a) Choi, C. L.; Alivisatos, A. P. From Artificial Atoms to Nanocrystal Molecules: Preparation and Properties of More Complex Nanostructures. *Annu. Rev. Phys. Chem.* **2010**, *61*, 369−389. (b) Salunkhe, A. B.; Khot, V. M.; Pawar, S. H. Magnetic Hyperthermia with Magnetic Nanoparticles: A Status Review. *Curr. Top. Med. Chem.* **2014**, *14*, 572−594. (c) Ubale, A. U.; Choudhari, D. M.; Kantale, J. S.; Mitkari, V. N.; Nikam, M. S.; Gawande, W. J.; Patil, P. P. Synthesis of nanostructured Cu$_x$S thin films by chemical route at room temperature and investigation of their size dependent physical properties. *J. Alloys Compd.* **2011**, *509*, 9249−9254.

(12) Sutorik, A. C.; Kanatzidis, M. G. Synthesis of [U(Se$_2$)$_4$]$^{4-}$ - the First Homoleptic Actinide Polychalcogenide Complex. *J. Am. Chem. Soc.* **1991**, *113*, 7754−7755.

(13) Sutorik, A. C.; Kanatzidis, M. G. Isolation of the polysulfide complex [(UO$_2$)(S$_2$)$_3$]$^{4-}$ from the in situ formation and subsequent reaction of uranyl cations in molten alkali metal polysulfide salts. *Polyhedron* **1997**, *16*, 3921−3927.

(14) (a) Behrle, A. C.; Kerridge, A.; Walensky, J. R. Dithio- and Diselenophosphinate Thorium(IV) and Uranium(IV) Complexes: Molecular and Electronic Structures, Spectroscopy, and Transmetalation Reactivity. *Inorg. Chem.* **2015**, *54*, 11625−11636. (b) Crawford, M. J.; Karaghiosoff, K.; Mayer, P. The Homoleptic U(NCSe)$_8^{4-}$ Anion in (Pr$_4$N)$_4$U(NCSe)$_8$·2CFCl$_3$ and Th(NCSe)$_4$(OP(NMe$_2$)$_3$)$_4$·0.5CH$_3$CN·0.5H$_2$O: First Structurally Characterised Actinide Isoselenocyanates. *Z. Anorg. Allg. Chem.* **2010**, *636*, 1903−1906. (c) Behrle, A. C.; Levin, J. R.; Kim, J. E.; Drewett, J. M.; Barnes, C. L.; Schelter, E. J.; Walensky, J. R. Stabilization of M-IV = Ti, Zr, Hf, Ce, and Th using a selenium bis(phenolate) ligand. *Dalton Trans* **2015**, *44*, 2693−2702. (d) Settineri, N. S.; Garner, M. E.; Arnold, J. A Thorium Chalcogenolate Series Generated by Atom Insertion into Thorium-Carbon Bonds. *J. Am. Chem. Soc.* **2017**, *139*, 6261−6269.

(15) Klapotke, T. M.; Krumm, B.; Polborn, K. Synthesis, chemistry, and characterization of perfluoroaromatic selenium derivatives. *Eur. J. Inorg. Chem.* **1999**, *1999*, 1359−1366.

(16) (a) Perdew, J. P.; Burke, K.; Ernzerhof, M. Generalized gradient approximation made simple. *Phys. Rev. Lett.* **1996**, *77*, 3865−3868. (b) Perdew, J. P.; Burke, K.; Ernzerhof, M. Generalized gradient approximation made simple. *Phys. Rev. Lett.* **1997**, *78*, 1396−1396. (c) Adamo, C.; Barone, V. Toward chemical accuracy in the computation of NMR shieldings: the PBE0 model. *Chem. Phys. Lett.* **1998**, *298*, 113−119.

(17) Grimme, S.; Antony, J.; Ehrlich, S.; Krieg, H. A consistent and accurate ab initio parametrization of density functional dispersion correction (DFT-D) for the 94 elements H-Pu. *J. Chem. Phys.* **2010**, *132*, 154104.

(18) Grimme, S.; Ehrlich, S.; Goerigk, L. Effect of the Damping Function in Dispersion Corrected Density Functional Theory. *J. Comput. Chem.* **2011**, *32*, 1456−1465.

(19) *Turbomole, version 7.0.2*; University of Karlsruhe and Forschungszentrum Karlsruhe, 1989−2007, TURBOMOLE GmbH since 2007. Available from http://www.turbomole.com (accessed on May 1, 2018).

(20) (a) Cao, X. Y.; Dolg, M. Segmented contraction scheme for small-core actinide pseudopotential basis sets. *J. Mol. Struct.: THEOCHEM* **2004**, *673*, 203−209. (b) Andrae, D.; Haeussermann,

DOI: 10.1021/acs.inorgchem.8b02555
Inorg. Chem. XXXX, XXX, XXX−XXX

U.; Dolg, M.; Stoll, H.; Preuss, H. Energy-adjusted *ab initio* pseudopotentials for the second and third row transition elements. *Theor. Chim. Acta* **1990**, *77*, 123−141. (c) Bergner, A.; Dolg, M.; Kuchle, W.; Stoll, H.; Preuss, H. *Ab-initio* Energy-Adjusted Pseudopotentials for Elements of Groups 13−17. *Mol. Phys.* **1993**, *80*, 1431−1441.

(21) Weigend, F.; Ahlrichs, R. Balanced basis sets of split valence, triple zeta valence and quadruple zeta valence quality for H to Rn: Design and assessment of accuracy. *Phys. Chem. Chem. Phys.* **2005**, *7*, 3297−3305.

(22) *Amsterdam Density Functional (ADF), version 2017.112*; SCM, Theoretical Chemistry, Vrije Univeriteit: Amsterdam, Netherlands, 2018. Available from http://www.scm.com (accessed on May 1, 2018).

(23) (a) Hrobarik, P.; Hrobarikova, V.; Greif, A. H.; Kaupp, M. Giant Spin-Orbit Effects on NMR Shifts in Diamagnetic Actinide Complexes: Guiding the Search of Uranium(VI) Hydride Complexes in the Correct Spectral Range. *Angew. Chem., Int. Ed.* **2012**, *51*, 10884−10888. (b) Greif, A. H.; Hrobarik, P.; Autschbach, J.; Kaupp, M. Giant spin-orbit effects on ^{1}H and ^{13}C NMR shifts for uranium(VI) complexes revisited: role of the exchange-correlation response kernel, bonding analyses, and new predictions. *Phys. Chem. Chem. Phys.* **2016**, *18*, 30462−30474. (c) Seaman, L. A.; Hrobarik, P.; Schettini, M. F.; Fortier, S.; Kaupp, M.; Hayton, T. W. A Rare Uranyl (VI)−Alkyl Ate Complex $[Li(DME)_{1.5}]_2[UO_2(CH_2SiMe_3)_4]$ and Its Comparison with a Homoleptic Uranium (VI)−Hexaalkyl. *Angew. Chem., Int. Ed.* **2013**, *52*, 3259−3263. (d) Pedrick, E. A.; Hrobarik, P.; Seaman, L. A.; Wu, G.; Hayton, T. W. Synthesis, structure and bonding of hexaphenyl thorium (IV): observation of a non-octahedral structure. *Chem. Commun.* **2016**, *52*, 689−692. (e) Greif, A. H.; Hrobarik, P.; Kaupp, M. Insights into *trans*-Ligand and Spin-Orbit Effects on Electronic Structure and Ligand NMR Shifts in Transition-Metal Complexes. *Chem. - Eur. J.* **2017**, *23*, 9790−9803. (f) Hrobarik, P.; Hrobarikova, V.; Meier, F.; Repisky, M.; Komorovsky, S.; Kaupp, M. Relativistic Four-Component DFT Calculations of ^{1}H NMR Chemical Shifts in Transition-Metal Hydride Complexes: Unusual High-Field Shifts Beyond the Buckingham-Stephens Model. *J. Phys. Chem. A* **2011**, *115*, 5654−5659.

(24) (a) Wolff, S. K.; Ziegler, T. Calculation of DFT-GIAO NMR shifts with the inclusion of spin-orbit coupling. *J. Chem. Phys.* **1998**, *109*, 895−905. (b) Wolff, S. K.; Ziegler, T.; van Lenthe, E.; Baerends, E. J. Density functional calculations of nuclear magnetic shieldings using the zeroth-order regular approximation (ZORA) for relativistic effects: ZORA nuclear magnetic resonance. *J. Chem. Phys.* **1999**, *110*, 7689−7698.

(25) Klamt, A.; Schuurmann, G. Cosmo - a New Approach to Dielectric Screening in Solvents with Explicit Expressions for the Screening Energy and Its Gradient. *J. Chem. Soc., Perkin Trans. 2* **1993**, *2*, 799−805.

(26) For recent examples of using QTAIM delocalization index as a descriptor of bond covalency, see also: (a) Rocchigiani, L.; Fernandez-Cestau, J.; Chambrier, I.; Hrobarik, P.; Bochmann, M. Unlocking Structural Diversity in Gold (III) Hydrides: Unexpected Interplay of *cis/trans*-Influence on Stability, Insertion Chemistry and NMR Chemical Shifts. *J. Am. Chem. Soc.* **2018**, *140*, 8287−8302. (b) Smiles, D. E.; Wu, G.; Hrobarik, P.; Hayton, T. W. Synthesis, Thermochemistry, Bonding, and ^{13}C NMR Chemical Shift Analysis of a Phosphorano-Stabilized Carbene of Thorium. *Organometallics* **2017**, *36*, 4519−4524. (c) Greif, A. H.; Hrobarik, P.; Hrobarikova, V.; Arbuznikov, A. V.; Autschbach, J.; Kaupp, M. A Relativistic Quantum-Chemical Analysis of the trans Influence on ^{1}H NMR Hydride Shifts in Square-Planar Platinum(II) Complexes. *Inorg. Chem.* **2015**, *54*, 7199−7208.

(27) (a) Te Velde, G.; Bickelhaupt, F. M.; Baerends, E. J.; Fonseca Guerra, C.; van Gisbergen, S. J. A.; Snijders, J. G.; Ziegler, T. Chemistry with ADF. *J. Comput. Chem.* **2001**, *22*, 931−967. (b) Hopffgarten, M. v.; Frenking, G. Energy decomposition analysis. *WIREs Comput. Mol. Sci.* **2012**, *2*, 43−62.

(28) *GADDS v.4.1.51, Data collection and rocking curve creation*; Bruker, 2015.

(29) *JADE7 v.7.0.6, Data display and graphics*; MDI, 2004.

(30) Bruker-AXS Inc., Madison, WI, USA.

(31) (a) Sheldrick, G. M. A short history of SHELX. *Acta Crystallogr., Sect. A: Found. Crystallogr.* **2008**, *64* (1), 112−120. (b) Sheldrick, G. M. Crystal structure determination with SHELX. *Acta Crystallogr., Sect. A: Found. Adv.* **2015**, *71*, 3−8. (c) Sheldrick, G. M. *SHELXS v.2013/1 and SHELXL v.2013/4, Programs for Crystal Structure Analysis*; University of Göttingen, Göttingen, Germany, 2013.

(32) Macrae, C. F.; Edgington, P. R.; McCabe, P.; Pidcock, E.; Shields, G. P.; Taylor, R.; Towler, M.; van De Streek, J. Mercury: visualization and analysis of crystal structures. *J. Appl. Crystallogr.* **2006**, *39*, 453−457.

(33) (a) Gotthelf, G.; Stuber, M. A.; Kornienko, A. Y.; Emge, T. J.; Brennan, J. G. Organosoluble tetravalent actinide di- and trifluorides. *Chem. Commun.* **2018**, *54*, 12018−12020. (b) Cooper, O. J.; Mills, D. P.; Lewis, W.; Blake, A. J.; Liddle, S. T. Reactivity of the uranium(IV) carbene complex $[U(BIPM^{TMS})(Cl)(\mu\text{-}Cl)_2Li(THF)_2]$ (BIPMTMS = $\{C(PPh_2NSiMe_3)_2\}$) towards carbonyl and heteroallene substrates: metallo-Wittig, adduct formation, C−F bond activation, and [2 + 2]-cycloaddition reactions. *Dalton Trans* **2014**, *43*, 14275−14283. (c) Berthet, J. C.; Thuery, P.; Ephritikhine, M. CCDC 959209. *CSD Commun.* **2013**. (d) Siffredi, G.; Berthet, J. C.; Thuery, P.; Ephritikhine, M. CCDC 958347. *CSD Commun.* **2013**.

(34) Barnhart, D. M.; Clark, D. L.; Gordon, J. C.; Huffman, J. C.; Watkin, J. G. Oligomerization of Metal-Oxygen Bonds in Thorium Alkoxide Chemistry: X-Ray Crystal Structures of $Th_4(O\text{-}i\text{-}Pr)_{16}(py)_2$ and $Th_2(OCHEt_2)_8(py)_2$. *Inorg. Chem.* **1994**, *33*, 3939−3944.

(35) Evans, W. J.; Walensky, J. R.; Ziller, J. W. Reactivity of Methyl Groups in Actinide Metallocene Amidinate and Triazenido Complexes with Silver and Copper Salts. *Organometallics* **2010**, *29*, 101−107.

(36) Travia, N. E.; Monreal, M. J.; Scott, B. L.; Kiplinger, J. L. Thorium-mediated ring-opening of tetrahydrofuran and the development of a new thorium starting material: preparation and chemistry of $ThI_4(DME)_2$. *Dalton Trans* **2012**, *41*, 14514−14523.

(37) Barnhart, D. M.; Clark, D. L.; Gordon, J. C.; Huffman, J. C.; Watkin, J. G.; Zwick, B. D. Solution Study of the Ambient-Temperature Monomer-Dimer Equilibrium $Th_2(OR)_8 \rightleftharpoons 2Th(OR)_4$ (R = CH-*i*-$Pr_2)_4$(quin)and X-Ray Crystal-Structures of $Th_2(OCH\text{-}i\text{-}Pr_2)_8$, $Th(OCH\text{-}i\text{-}Pr_2)_4$(quin), and $ThI(OCH\text{-}i\text{-}Pr_2)_3(py)_2$. *Inorg. Chem.* **1995**, *34*, 5416−5423.

(38) Edelman, M. A.; Hitchcock, P. B.; Hu, J.; Lappert, M. F. Organoactinide Chemistry.II. The Chemistry of Some Novel Cyclopentadienylthorium Complexes. *New J. Chem.* **1995**, *19*, 481−489.

(39) Yang, P.; Zhou, E.; Hou, G.; Zi, G.; Ding, W.; Walter, M. D. Experimental and Computational Studies on the Formation of Thorium-Copper Heterobimetallics. *Chem. - Eur. J.* **2016**, *22*, 13845−13849.

(40) Hohloch, S.; Garner, M. E.; Parker, B. F.; Arnold, J. New supporting ligands in actinide chemistry: tetramethyltetraazaannulene complexes with thorium and uranium. *Dalton Trans* **2017**, *46*, 13768−13782.

(41) (a) Cantat, T.; Scott, B. L.; Kiplinger, J. L. Convenient access to the anhydrous thorium tetrachloride complexes $ThCl_4(DME)_2$, $ThCl_4$(1,4-dioxane)$_2$ and $ThCl_4(THF)_{3.5}$ using commercially available and inexpensive starting materials. *Chem. Commun.* **2010**, *46*, 919−921. (b) Ward, A. L.; Lukens, W. W.; Lu, C. C.; Arnold, J. Photochemical Route to Actinide-Transition Metal Bonds: Synthesis, Characterization and Reactivity of a Series of Thorium and Uranium Heterobimetallic Complexes. *J. Am. Chem. Soc.* **2014**, *136*, 3647−3654. (c) Fang, B.; Hou, G.; Zi, G.; Ding, W.; Walter, M. D. Steric and Electronic Influences of Internal Alkynes on the Formation of Thorium Metallacycles: A Combined Experimental and Computational Study. *Organometallics* **2016**, *35*, 1384−1391. (d) Rickard, C. E. F.; Woollard, D. C. Structure of Tetrachlorotetrakis(Diphenyl

DOI: 10.1021/acs.inorgchem.8b02555
Inorg. Chem. XXXX, XXX, XXX−XXX

Sulfoxide)Thorium(IV). *Acta Crystallogr., Sect. B: Struct. Crystallogr. Cryst. Chem.* **1980**, *36*, 292−294. (e) Moloy, K. G.; Marks, T. J.; Day, V. W. Carbon-Monoxide Activation by Organoactinides. η^2-Acyl-CO Coupling and the Formation of Metal-Bound Ketenes. *J. Am. Chem. Soc.* **1983**, *105*, 5696−5698. (f) Mora, E.; Maria, L.; Biswas, B.; Camp, C.; Santos, I. C.; Pecaut, J.; Cruz, A.; Carretas, J. M.; Marcalo, J.; Mazzanti, M. Diamine Bis(phenolate) as Supporting Ligands in Organoactinide(IV) Chemistry. Synthesis, Structural Characterization, and Reactivity of Stable Dialkyl Derivatives. *Organometallics* **2013**, *32*, 1409−1422. (g) Stobbe, B. C.; Powell, D. R.; Thomson, R. K. Schiff base thorium(IV) and uranium(IV) chloro complexes: synthesis, substitution and oxidation chemistry. *Dalton Trans* **2017**, *46*, 4888−4892. (h) Karmel, I. S. R.; Fridman, N.; Eisen, M. S. Actinide Amidinate Complexes with a Dimethylamine Side Arm: Synthesis, Structural Characterization, and Reactivity. *Organometallics* **2015**, *34*, 636−643.

(42) Alvarez, S.; Hoffmann, R.; Mealli, C. A Bonding Quandary-or-A Demonstration of the Fact That Scientists Are Not Born With Logic. *Chem. - Eur. J.* **2009**, *15*, 8358−8373.

(43) (a) Fagin, A. A.; Kuznetsova, O. V.; Balashova, T. V.; Cherkasov, A. V.; Fukin, G. K.; Bochkarev, M. N. Iodide-sulfides of dysprosium: Elucidation of the pathway to lanthanide iodide-sulfide-nitride clusters. *Inorg. Chim. Acta* **2018**, *469*, 227−230. (b) Zhang, Z. X.; Zhang, L. X.; Li, Y. R.; Hong, L. C.; Chen, Z. X.; Zhou, X. G. Activation of Bis(guanidinate)lanthanide Alkyl and Aryl Complexes on Elemental Sulfur: Synthesis and Characterization of Bis-(guanidinate)lanthanide Thiolates and Disulfides. *Inorg. Chem.* **2010**, *49*, 5715−5722.

(44) (a) Melman, J. H.; Fitzgerald, M.; Freedman, D.; Emge, T. J.; Brennan, J. G. Chalcogen-rich lanthanide clusters from lanthanide halide starting materials: A new approach to the low-temperature synthesis of LnS_x solids from molecular precursors. *J. Am. Chem. Soc.* **1999**, *121*, 10247−10248. (b) Fitzgerald, M.; Emge, T. J.; Brennan, J. G. Chalcogen-rich lanthanide clusters with fluorinated thiolate ligands. *Inorg. Chem.* **2002**, *41*, 3528−3532.

(45) (a) Brunner, H.; Meier, W.; Wachter, J.; Guggolz, E.; Zahn, T.; Ziegler, M. L. Investigation into the Reactivity of the Metal-Metal Triple Bond in $[Cp'(CO)_2M]_2$($Cp'=\eta^5$-C_5Me_5; M = Mo,W) vs. Elemental Sulfur. Formation of Different $Cp'_2M_2S_4$ Isomers and Crystal Structures of $Cp'_2Mo_2(\mu\text{-}S_2)$ $(\mu\text{-}S)_2$ and $Cp'_2(CO)_2W_2(\mu\text{-}S)_2S$. *Organometallics* **1982**, *1*, 1107−1113. (b) Fedin, V. P.; Muller, A.; Filipek, K.; Rohlfing, R.; Bogge, H.; Vorovets, A. V.; Dziegielewski, J. O. Extrusion of Molecular Clusters from Solid-State Materials - Synthesis by Application of γ-Irradiation - Molecular and Crystal-Structure of $(H_9O_4)(Et_4N)[MO_3S_7Br_6]$. *Inorg. Chim. Acta* **1994**, *223*, 5−7. (c) Bar-Nahum, I.; York, J. T.; Young, V. G.; Tolman, W. B. Novel reactivity of side-on (disulfido)dicopper complexes supported by Bi- and tridentate nitrogen donors: Impact of axial coordination. *Angew. Chem., Int. Ed.* **2008**, *47*, 533−536. (d) Kubas, G. J.; Ryan, R. R.; Kubatmartin, K. A. Cleavage of SO_2 on $(\eta^5\text{-}C_5Me_5)_2Mo_2(\mu\text{-}S_2)(\mu\text{-}S)_2$ to Form S_8 and a Thiosulfate Complex, $(\eta^5\text{-}C_5Me_5)_2Mo_2(\mu\text{-}S_2)(\mu\text{-}S)(\mu\text{-}SSO_3)$ - Possible Role in Homogeneous Hydrogenation of SO_2 Catalyzed by Mo-S Complexes. *J. Am. Chem. Soc.* **1989**, *111*, 7823−7832. (e) Fujisawa, K.; Morooka, Y.; Kitajima, N. Formation of a μ-η^2:η^2-Disulfide Dinuclear Copper(II) Complex by Thermal-Decomposition of a Thiolate Complex via C-S Bond-Cleavage. *J. Chem. Soc., Chem. Commun.* **1994**, 623−624. (f) Helton, M. E.; Maiti, D.; Zakharov, L. N.; Rheingold, A. L.; Porco, J. A.; Karlin, K. D. A μ-η^2:η^2-disulfide dicopper(II) complex from reaction of S_8 with a copper(I) precursor: Reactivity of the bound disulfur moiety. *Angew. Chem., Int. Ed.* **2006**, *45*, 1138−1141. (g) Kajita, Y.; Matsumoto, J.; Takahashi, I.; Hirota, S.; Funahashi, Y.; Ozawa, T.; Masuda, H. Syntheses, characterization, and reactivities of (μ-η^2:η^2)-disulfido)-dicopper(II) complexes with N-alkylated *cis, cis*-1,3,5-triaminocyclohexane derivatives. *Eur. J. Inorg. Chem.* **2008**, *2008*, 3977−3986. (h) Ryu, S.; Whang, D.; Kim, H. J.; Kim, K.; Yoshida, M.; Hashimoto, K.; Tatsumi, K. Novel disulfido- and diselenido-bridged zirconium and hafnium porphyrin dimers with unusual coordination geometries: $[M(TPP)]_2(\mu\text{-}\eta^2\text{-}Q_2)_2$ (M = Zr, Hf; Q = S, Se). *Inorg. Chem.* **1997**, *36*, 4607−4609.

(46) (a) Huebner, L.; Kornienko, A.; Emge, T. J.; Brennan, J. G. Lanthanide clusters with internal Ln: Fragmentation and the formation of dimers with bridging Se^{2-} and Se_2^{2-} ligands. *Inorg. Chem.* **2005**, *44*, 5118−5122. (b) Kornienko, A. Y.; Emge, T. J.; Brennan, J. G. Chalcogen-rich lanthanide clusters: Cluster reactivity and the influence of ancillary ligands on structure. *J. Am. Chem. Soc.* **2001**, *123*, 11933−11939.

(47) (a) Yao, S. L.; Xiong, Y.; Zhang, X. H.; Schlangen, M.; Schwarz, H.; Milsmann, C.; Driess, M. Facile Dissociation of $[(LNi^{II})_2E_2]$ Dichalcogenides: Evidence for $[LNi^{II}E_2]$ Superselenides and Supertellurides in Solution. *Angew. Chem., Int. Ed.* **2009**, *48*, 4551−4554. (b) Wu, D. H.; Xu, B. H.; Li, Y. Z.; Yan, H. Diruthenium half-sandwich complexes containing one μ-E_2 (E = S, Se) unit and two chelating 1,2-dicarba-closo-dodecaborane-1,2-dithiolate ligands: Reactivity studies with methyl acetylene carboxylates. *Organometallics* **2007**, *26*, 6300−6306. (c) Fedin, V. P.; Sokolov, M. N.; Gerasko, O. A.; Virovets, A. V.; Podberezskaya, N. V.; Fedorov, V. Y. Triangular $M_3Se_7^{4+}$ and $M_3Se_4^{4+}$Complexes (M = Mo, W). An X-Ray Study of $Mo_3Se_7(Et_2NCS_2)_4$ and $W_3Se_7(Et_2NCS_2)_4$. *Inorg. Chim. Acta* **1991**, *187*, 81−90. (d) Bereau, V.; Ibers, J. A. Synthesis and characterization by diffraction and ^{31}P- and ^{77}Se-NMR spectroscopy of $[Mo_3(\mu_3\text{-}Se)(\mu_2\text{-}Se_2)_3\{N(SePPh_2)_3\}_3]$ Br and $[Mo_3(\mu_3\text{-}Se)$ $(\mu_2\text{-}Se_2)_3\{Se_2P\text{-}(OCH_2CH_3)_2\}_3]$ Br. *Cr. Acad. Sci. II C* **2000**, *3*, 123−129.

(48) Bondi, A. Van der Waals Volumes and Radii. *J. Phys. Chem.* **1964**, *68*, 441−451.

(49) (a) Kornienko, A.; Melman, J. H.; Hall, G.; Emge, T. J.; Brennan, J. G. Chalcogen Rich Lanthanide Clusters from Halide Starting Materials (II): Selenido Compounds. *Inorg. Chem.* **2002**, *41*, 121−126. (b) Kornienko, A.; Moore, B. F.; Kumar, G. A.; Tan, M.-C.; Riman, R. E.; Brik, M. G.; Emge, T. J.; Brennan, J. G. Highly NIR-Emissive Lanthanide Polyselenides. *Inorg. Chem.* **2011**, *50*, 9184−9190. (c) Kornienko, A.; Emge, T. J.; Kumar, G. A.; Riman, R. E.; Brennan, J. G. Lanthanide Clusters with Internal Ln Ions: Highly Emissive Molecules with Solid-State Cores. *J. Am. Chem. Soc.* **2005**, *127*, 3501−3505. (d) Moore, B. F.; Kumar, G. A.; Tan, M.-C.; Kohl, J.; Riman, R. E.; Brik, M. G.; Emge, T. J.; Brennan, J. G. Lanthanide Clusters with Chalcogen Encapsulated Ln: NIR Emission from Nanoscale $NdSe_x$. *J. Am. Chem. Soc.* **2011**, *133*, 373−378.

(50) Freedman, D.; Emge, T. J.; Brennan, J. G. Chalcogen-Rich Lanthanide Clusters: Compounds with Te^{2-}, $(TeTe)^{2-}$, TePh, TeTePh, $(TeTeTe(Ph)TeTe)^{5-}$, and $[(TeTe)_4TePh]^{9-}$ Ligands; Single Source Precursors to Solid-State Lanthanide Tellurides. *Inorg. Chem.* **2002**, *41*, 492−500.

(51) (a) Bueyuekyazi, M.; Fischer, T.; Yu, P.; Coll, M.; Mathur, S. A cobalt(II)heteroarylalkenolate precursor for homogeneous Co_3O_4 coatings by atomic layer deposition. *Dalton Trans* **2017**, *46*, 12996−13001. (b) Jamil, A.; Schlaefer, J.; Goenuellue, Y.; Lepcha, A.; Mathur, S. Precursor-Derived Rare Earth Metal Pyrochlores: $Nd_2Sn_2O_7$ Nanofibers and Thin Films As Efficient Photoabsorbers. *Cryst. Growth Des.* **2016**, *16*, 5260−5267. (c) Lee, J.; Brewer, M.; Berardini, M.; Brennan, J. G. Trivalent Lanthanide Chalcogenolates - Synthesis, Structure, and Thermolysis Chemistry. *Inorg. Chem.* **1995**, *34*, 3215−3219. (d) Fuhrmann, D.; Dietrich, S.; Krautscheid, H. Copper Zinc Thiolate Complexes as Potential Molecular Precursors for Copper Zinc Tin Sulfide (CZTS). *Chem. - Eur. J.* **2017**, *23*, 3338−3346. (e) Gaber, A. A. M.; Wentrup, C. Pyrolysis of hydrazine derivatives and related compounds with N-N single bonds. *J. Anal. Appl. Pyrolysis* **2017**, *125*, 258−278. (f) Holligan, K.; Rogler, P.; Rehe, D.; Pamula, M.; Kornienko, A. Y.; Emge, T. J.; Krogh-Jespersen, K.; Brennan, J. G. Copper, Indium, Tin, and Lead Complexes with Fluorinated Selenolate Ligands: Precursors to MSe_x. *Inorg. Chem.* **2015**, *54*, 8896−8904.

(52) D'Eye, R. W. M. The crystal structures of $ThSe_2$ and Th_7Se_{12}. *J. Chem. Soc.* **1953**, 1670−1672.

DOI: 10.1021/acs.inorgchem.8b02555
Inorg. Chem. XXXX, XXX, XXX−XXX